



**HAL**  
open science

## Genome-wide expression analysis id 1 entifies core components during iron starvation in hexaploid wheat

Gazaldeep Kaur, Vishnu Shukla, Anil Kumar, Mandeep Kaur, Parul Goel, Palvinder Singh, Anuj Shukla, Jaspreet Kaur, Jagtar Singh, Shrikant Mantri, et al.

### ► To cite this version:

Gazaldeep Kaur, Vishnu Shukla, Anil Kumar, Mandeep Kaur, Parul Goel, et al.. Genome-wide expression analysis id 1 entifies core components during iron starvation in hexaploid wheat. 2019. hal-02786468

**HAL Id: hal-02786468**

**<https://hal.inrae.fr/hal-02786468>**

Preprint submitted on 5 Jun 2020

**HAL** is a multi-disciplinary open access archive for the deposit and dissemination of scientific research documents, whether they are published or not. The documents may come from teaching and research institutions in France or abroad, or from public or private research centers.

L'archive ouverte pluridisciplinaire **HAL**, est destinée au dépôt et à la diffusion de documents scientifiques de niveau recherche, publiés ou non, émanant des établissements d'enseignement et de recherche français ou étrangers, des laboratoires publics ou privés.



Distributed under a Creative Commons Attribution 4.0 International License

1 **Integrative analysis of hexaploid wheat roots identifies signature**  
2 **components during iron starvation**

3

4 Gazaldeep Kaur<sup>1,2\*</sup>, Vishnu Shukla<sup>1,3\*</sup>, Anil Kumar<sup>1,2</sup>, Mandeep Kaur<sup>1,2</sup>, Parul Goel<sup>1</sup>,  
5 Palvinder Singh<sup>1</sup>, Anuj Shukla<sup>1</sup>, Varsha Meena<sup>1</sup>, Jaspreet Kaur<sup>3</sup>, Jagtar Singh<sup>2</sup>, Shrikant  
6 Mantri<sup>1</sup>, Hatem Rouached<sup>4</sup> and Ajay Kumar Pandey<sup>1#</sup>

7

8

9 Author affiliations

10 <sup>1</sup>National Agri-Food Biotechnology Institute (Department of Biotechnology), Sector 81,  
11 Knowledge City, Mohali-140306, Punjab, India.

12 <sup>2</sup>Department of Biotechnology, Panjab University, Chandigarh, India.

13 <sup>3</sup>University Institute of Engineering and Technology, Panjab University, Chandigarh, India

14 <sup>4</sup>BPMP, Université de Montpellier, INRA, CNRS, Montpellier SupAgro, 34060  
15 Montpellier, France.

16

17 *\*Authors contributed equally*

18 *#Corresponding author*

19 Dr. Ajay K Pandey, Scientist-E.

20 National Agri-Food Biotechnology Institute (Department of Biotechnology), Sector 81,  
21 Knowledge City, Mohali-140306, Punjab, India.

22 Telephone: +91-1724990124

23 Email: pandeyak@nabi.res.in; pandeyak1974@gmail.com

24 ORCID iD: <https://orcid.org/0000-0003-1064-139X>

25

26 **Running Title:** Fe starvation response in hexaploid wheat roots

27 **Highlight:** During Fe starvation, wheat roots show prolific expression of core components  
28 involved in Strategy-II mode of Fe uptake along with significant changes in the metabolome  
29 including enhanced GST activity.

30

31

32

33

34 **Abstract**

35 Iron is an essential micronutrient for all organisms. In crop plants, iron deficiency can  
36 decrease crop yield significantly, however our current understanding of how major crops  
37 respond to iron deficiency remains limited. Herein, the effect of Fe deprivation at both the  
38 transcriptomic and metabolic levels in hexaploid wheat was investigated. Genome-wide gene  
39 expression reprogramming was observed in wheat roots subjected to Fe starvation, with a  
40 total of 5854 genes differential expressed. Homoeolog and subgenome specific analysis  
41 unveiled induction bias contribution from the A and B genomes. In general, the  
42 predominance of genes encoding for nicotianamine synthase, yellow stripe like transporters,  
43 metal transporters, ABC transporters and zinc-induced facilitator-like protein was noticed.  
44 Expression of genes related to the strategy-II mode of Fe uptake was predominant as well.  
45 Our transcriptomic data were in agreement with the GC-MS analysis that showed the  
46 enhanced accumulation of various metabolites such as fumarate, malonate, succinate and  
47 xylofuranose, which could be contributing to Fe-mobilization. Interestingly, Fe starvation  
48 leads to significant temporal increase of glutathione-S-transferase both at transcriptional and  
49 in enzymatic activity levels, which indicates the involvement of glutathione in response to Fe  
50 stress in wheat roots. Taken together, our result provides new insight into the wheat response  
51 to Fe starvation at molecular level and lays foundation to design new strategies for the  
52 improvement of Fe nutrition in crops.

53

54 **Key words:** iron starvation, *Triticum aestivum*, glutathione metabolism, transcriptome, gene  
55 expression, genome bias.

56

57

58

59

60

61

62

63

64

65

66

67

## 68 **Introduction**

69 Iron (Fe) is among the essential micronutrients in plants that participate as catalytic cofactors  
70 in several key processes including photosynthesis, respiration, chlorophyll biosynthesis, and  
71 nitrogen fixation (Kim and Rees, 1992; Morrissey and Guerinot, 2009; Li et al., 2017). The  
72 bioavailability of Fe in the soil is strongly dependant on its solubility, aerobic and calcareous  
73 soil condition, pH, and the presence of natural ligands secreted by plant roots (Marschner H.,  
74 1995; Morrissey and Guerinot, 2009; Thomine et al., 2013). To circumvent the above  
75 challenges for Fe uptake by the roots, plants have adapted two modes of uptake strategies.  
76 Strategy-I, mostly predominant in Eudicot species, primarily relies on the enrichment of  
77 rhizospheric regions with protons ( $H^+$ ) and other reducing agents (Hell and Stephan, 2003;  
78 Santi et al., 2005; Santi and Schmidt 2009; Kobayashi and Nishizawa 2012). In contrast,  
79 graminaceous species follow the Strategy-II mode of uptake, which involves the transport of  
80 Fe in the complex-chelated form (Mori et al., 1999; Kobayashi and Nishizawa, 2012;  
81 Connorton et al., 2017). The primary components involved in chelation are the  
82 phytosiderophores (PS) secreted by plant cells in the rhizospheric region mainly by efflux  
83 transporters (Morrissey and Gueirnot, 2009; Kobayashi and Nishizawa, 2012). One of the  
84 main components of these secreted siderophores involved in Fe chelation is referred to as  
85 mugineic acids (MAs). The transporters involved in the secretion of the MAs are identified as  
86 transporter of mugineic (TOM) acid proteins (Nozoye et al., 2011). The complex chelated  
87 form of  $Fe^{3+}$ -PS is taken up by the specific root transporter referred to as yellow stripe-like  
88 transporter proteins (YSL) (Curie et al., 2001; Gross et al., 2003, Yordem et al., 2011).  
89 Subsequently, Fe is transported in the plant organelles by multiple partners including  
90 specialized long distance, tissue-specific transporters as reported in monocots (e.g rice,  
91 maize) and eudicots (e.g. Arabidopsis) (Kim et al., 2006; Waters et al., 2011). In other  
92 monocots such as maize and rice, the presence of genetic components for both Strategy-I and  
93 II were reported (Ishimaru et al., 2006; Inoue et al., 2009; Lee et al., 2009; Zanin et al.,  
94 2017). At the metabolome level, analytical approaches utilizing GC-MC and LC-MS were  
95 utilized to study the components of Fe starvation in plants (Palmer et al., 2014; Kabir et al.,  
96 2013). However, the molecular and metabolic activity predominant for Fe uptake by the roots  
97 of hexaploid wheat still remains to be elucidated.

98         Microarrays have been successfully used to investigate the global transcriptional  
99 changes in Arabidopsis plants grown in Fe starved conditions (Thimm et al., 2001; Buckhout  
100 et al., 2009; Yang et al., 2010). Significant changes in the expression pattern of the genes  
101 primarily involved in Strategy-II mode of uptake were observed in roots of maize and rice

102 subjected to Fe-deficiency stress (Li et al., 2014; Quinet et al., 2012; Kobayashi et al., 2014;  
103 Bashir et al., 2014). The transcriptome analysis of Fe-starved plants is characterised by an  
104 important change in gene expression of several transcriptional regulators such as transcription  
105 factors (TFs) (Colangelo et al., 2004; Kobayashi et al., 2009; Long et al., 2010; Li et al.,  
106 2016; Connorton et al., 2017) or key genes related to phytohormone homeostasis (Schmidt et  
107 al., 2000; Hindt and Guerinot, 2012). Fe starvation also leads to changes in the abundance of  
108 transcripts related to plant metabolism and genes involved in signalling pathways that  
109 modulate nutrient uptake. Additionally, genes involved in ethylene/auxin signalling or linked  
110 with certain other macronutrients like nitrogen, sulphur and phosphorus are also significantly  
111 expressed (Romera et al., 1994; Zheng et al., 2009; Romera et al., 2011; Borlotti et al., 2012;  
112 Zuchi et al., 2015; Lin et al., 2016; Zanin et al., 2017; Garnica et al., 2018). Therefore,  
113 transcriptome analysis is a powerful approach to help understand the network involved in  
114 plants response to Fe.

115 Hexaploid wheat is an important crop that is also a good, affordable source of  
116 nutrition. Fe deficiency strongly affects the growth of cereal crops and productivity (Yousfi  
117 et al., 2009; Bocchini et al., 2015). The development of transcriptome technology such as  
118 RNA sequencing-RNAseq and the availability of genome sequence for hexaploid wheat  
119 (genome A, B, D) (International Wheat Genome Consortium, 2014) combined with  
120 metabolomic approaches will help improve our knowledge of wheat response to nutritional  
121 stress (e.g. -Fe) (Borrill et al., 2018). Our current knowledge on how the wheat genome  
122 responds to Fe limiting condition remains obscure and unanswered. In addition, how the  
123 different genomes could impact the homoeolog based expression of the transcripts,  
124 categorically under different stress conditions, remains to be explored (Ramirez-Gonzalez et  
125 al., 2018). In the current study, RNA-seq based approach was utilized to address the  
126 molecular components involved in wheat roots during Fe starved condition. Further, genome-  
127 based expression study was performed that provided preliminary clue on coordinated  
128 expression of the homoeologs. Metabolic profiling result support the data from the  
129 transcriptome study and pinpoint the role of glutathione mediated response. Collectively our  
130 results provide the first insight on molecular and biochemical responses of hexaploid wheat  
131 under Fe starvation.

132

### 133 **Materials and methods**

134 *Plant materials, starvation conditions and plant sampling*

135 Hexaploid bread wheat variety ‘C-306’ was used for the experimental purpose. Wheat grains  
136 were subjected to stratification in dark at 4 °C for overnight and were allowed to germinate  
137 for 5 days on the Petri plates containing 2-3 layers of wet Whatman filter paper. The  
138 endosperms were removed from the developing seedlings once they started browning.  
139 Subsequently, the seedlings were transferred in PhytaBox™ and grown for 7 days in  
140 Hoagland’s nutrient solution. A total of forty-eight seedlings were kept equally in four  
141 PhytaBoxes, used for each treatment. After 7 days, nutrient solutions were replaced on the  
142 basis of different treatments. For Fe starvation (-Fe) 2 μM Fe (III) EDTA was used as the Fe  
143 source. For control plants (+Fe) concentrations of nutrients were unchanged in above-  
144 mentioned Hoagland’s solution containing (20 μM Fe (III) EDTA). Treated seedlings were  
145 grown in the described medium for 20 days in a growth chamber set at 20±1 °C, 50-70%  
146 relative humidity and photon rate of 300 μmol quanta m<sup>-2</sup> s<sup>-1</sup> with 16 h day/8 h night  
147 cycle. For sampling, roots and shoots were collected at different time points after starvation  
148 (5, 10, 15 and 20 days). On the basis of distinct phenotype, samples collected at 20 days after  
149 starvation (DAS) were used for transcriptome analysis. A total of four biological replicates  
150 (each containing 10-12 seedlings) were used. Subsequently, RNA extractions were performed  
151 independently for each of the pools. Prior to RNA sequencing, quality of RNA was checked  
152 and extractions derived from two replicates were pooled together thereby generating two  
153 experimental samples for each of the respective conditions. Remaining samples were snap  
154 frozen in liquid nitrogen and stored at -80°C. To distinctively observe primary root and 1<sup>st</sup>  
155 order lateral root, individual plants were moved onto a 150 mm wide petri plate filled with  
156 distilled water and characteristics were manually examined. To ascertain root characteristics,  
157 6-8 wheat seedlings were used for each of the treatments with two experimental replicates.

158

#### 159 *RNA extraction and Illumina sequencing*

160 Total RNA was extracted from the treated root samples along with the control by Trizol  
161 (Invitrogen, ThermoFisher, USA) as per the manufacturer’s instruction. The quality and  
162 quantity were checked on the 1% denaturing RNA agarose gel and Nanodrop respectively.  
163 Subsequently, all the RNA used for library preparations were checked for their RNA integrity  
164 number ≥ 8.5 using Bioanalyzer (Agilent, USA). The quality control (QC) passed RNA  
165 samples were then processed for library preparation. The Paired-ended (PE) libraries were  
166 prepared from the total RNA using Illumina TruSeq stranded mRNA library prep kit as per  
167 the instructions (Illumina Inc., USA). The generated mean of the libraries fragment size  
168 distribution was 559 bp, 584 bp, 546 bp and 604 bp for the samples. The generated libraries

169 were sequenced on the NextSeq 500 using 2 X 150 bp chemistry. The raw reads were  
170 processed further before the sorted high-quality reads were mapped to the reference genome.

171

### 172 *RNA-Seq analysis*

173 Adapter clipping and quality trimming of the raw reads were performed using Trimmomatic-  
174 0.35. The sequenced raw reads were processed to obtain high quality clean reads. Ambiguous  
175 reads (reads with unknown nucleotides “N” larger than 5%) and low-quality sequences (more  
176 than 10% quality threshold QV<20 phred score) were removed. A minimum length of 100  
177 nts after trimming was applied. Finally, high-quality (QV>20), paired-end reads were used  
178 for reference based read mapping. The genome of *Triticum aestivum* L. was taken as  
179 reference for analysis. The Gene Feature Format files were downloaded from Ensembl Plants  
180 (TGACv1.37). The reads were mapped to the reference genome using TopHat v2.1.1 with  
181 default parameters. Cufflinks v2.2.1 program assembled the transcriptome data from RNA-  
182 seq data and quantified their expression. Mapped reads were subjected to Cufflinks, followed  
183 by Cuffmerge and Cuffdiff. Log2 Fold Change (FC) values greater than one was considered  
184 up-regulated whereas less than 1 were considered as down-regulated. These genes were  
185 further categorized on the basis of statistical significance ( $p < 0.05$ ) and the False Discovery  
186 Rate (FDR 0.05) after Benjamin-Hochberg corrections for multiple testing for their  
187 significant expression.

188 Comprehensive gene annotation of wheat sequences was done using KOBAS 3.0 (Xie  
189 et al., 2011) annotate module by alignment with Rice sequences (BLASTP, cutoff 1e-5).  
190 MapMan was used to visualize the pathways involving wheat differentially expressed genes  
191 (DEGs). Pathway enrichment analysis was performed using KOBAS standalone tool. MeV  
192 was used to construct heatmaps for selected DEGs using the normalized expression values of  
193 genes. The data generated from this study has been deposited in the NCBI Sequence Read  
194 Archive (SRA) database and is accessible with the submission ID- SUB5206887 and  
195 BioProjectID-PRJNA529036.

196

### 197 *Gene annotation filtering and functional enrichment analysis*

198 Significant sets of DEGs under iron starvation were further mapped using GO and MapMan.  
199 The GO annotation was downloaded from ensembl plants  
200 (<https://plants.ensembl.org/biomart/martview>). Mercator (Lohse et al., 2014) was used to  
201 build MapMan mapping file for TGACv1 sequences and DEGs were visualized in MapMan  
202 v3.1.1 tool (Thimm et al., 2004). For functional categorization of DEGs that were positively

203 and negatively correlated with iron starvation, BINGO version 3.0.3 (Maere et al., 2005) was  
204 used to perform GO enrichment analysis with hypergeometric test and significant terms with  
205 an FDR value below 0.05 were considered. For gene ontology mapping, GO\_full.obo  
206 ontology file was downloaded from GO consortium. MapMan classification was used to  
207 categorize DEGs into transcriptional factors. The results were visualized as network using  
208 EnrichmentMap version 2.2.1 (Merico et al., 2010) and gene expression overview in various  
209 pathways were visualized in MapMan tool.

210

### 211 *Homoeolog specific expression analysis for genome bias*

212 To identify wheat homoeologous triplets; ensembl biomart TGACv1 was used to extract all  
213 possible homoeologous relations. This led to 86830 pairwise homoeologous relations. An in-  
214 house script was used to select only the triplets where contribution from each genome was  
215 1:1:1 (A:B:D), thus generating 16850 triplets. Further, triplets resulting from potential  
216 translocation events were not considered, i.e., only homoeolog triplets from same  
217 chromosome (eg, 1A, 1B, 1D triplet is accepted, whereas, 2A, 3B, 3D is rejected) were taken  
218 for analysis. Finally, 15604 triplets (15604\*3 = 46812 genes) were used for studying genome  
219 induction biasness in response to iron stress. Paired end reads were aligned to the reference  
220 (selected scaffolds from genome that harbour 15604 triplets) using TopHat v2.1.1 with a  
221 specific argument (--b2-very-sensitive) (Powell et al., 2017), which leads to more stringent  
222 alignments as required for homoeologs. The Cufflinks pipeline was used to obtain FPKM  
223 values and differentially expressed genes.

224 Further, relative abundance levels and expression bias for homoeologs was studied by  
225 considering the homoeologous gene triplets with expression of FPKM  $\geq 1$  each in both the  
226 control as well as Fe starved conditions. For this, the normalised relative expression for each  
227 homoeolog within a triad was calculated. For example, the relative expression from A will be  
228 represented as:

$$Relative\ expression_A = \frac{FPKM_A}{FPKM_A + FPKM_B + FPKM_D}$$

229 Thus, relative expression levels of A, B and D homoeologs within each triad were calculated  
230 similarly. Seven homoeolog expression bias categories were defined as described earlier by  
231 Ramirez-Gonzalez et al., (2018). In total, seven categories defined as one balanced category  
232 and six unbalanced homoeolog-suppressed/homoeolog-dominant (from either of the  
233 genomes) were listed for the ideal relative expression of A, B and D. Euclidian distance  
234 (using cdist function from rdist package, R3.3.2) was calculated between normalised relative

235 expression for each triad and the seven ideal categories. The shortest distance was used as a  
236 deciding factor to group the triads into the seven respective categories.

237

### 238 *Quantitative real time-PCR (qRT-PCR)*

239 For validation of the gene expression, qRT-PCR analysis was performed. Total RNA (2 µg)  
240 isolated from the above experiments were used to validate the expression by using qRT-PCR  
241 method. Genomic DNA present in trace amount was removed by DNaseI treatment using a  
242 Turbo DNA-free kit (Invitrogen, ThermoFisher, USA). Further, cDNA was synthesized from  
243 two micrograms of DNA-free RNA using Superscript III first strand (Invitrogen,  
244 ThermoFisher, USA) with random hexamer primers following the manufacturer's guidelines.  
245 For qPCR reaction, gene-specific primers of each gene were designed from conserved  
246 regions of all three homeolog sequences (Supplementary Table S1). qRT-PCR was  
247 performed using QuantiTect SYBR Green RT-PCR mastermix (Qiagen, USA) with programs  
248 recommended by the manufacturer in the ABI 7700 sequence detector (Applied Biosystems,  
249 USA). ADP-ribosylation factor (ARF) and Actin were used as internal controls. Two  
250 independent experimental replicates with four technical replicates were performed for each  
251 sample. The relative amount of gene expression was calculated using  $2^{-\Delta\Delta CT}$  method.

252

### 253 *Metabolite extraction and GC-MS profiling*

254 Extraction of total metabolites was performed similarly as previously described (Wang et al.,  
255 2018). Roots of plants grown under -Fe and +Fe were sampled in triplicate manner and dried  
256 for 1 week. Each of 50 mg crushed samples was extracted in a mixture of solvents  
257 (precooled; 300 µl methanol, 30 µl 2 mg ml<sup>-1</sup> nonadecanoic acid methylester and 30 µl 0.2  
258 mg ml<sup>-1</sup> sorbitol) for 15 minutes (70°C, 1000rpm). Further, at room temperature 200 µl  
259 chloroform was added and shaken for 5 min (37°C, 1000rpm). To obtain phase separation,  
260 400 µl H<sub>2</sub>O was added to each sample, vortexed and centrifuged (10 min, 13,000 rpm). From  
261 the upper polar phase approximately 200 µl was finally aliquoted for complete drying.

262 For GC-MS analysis, metabolites were subjected to methoxyamination and  
263 trimethylsilylation. Dried polar phase were shaken for 1.5 hr at 30°C in 40 µl of MeOX (40  
264 mg ml<sup>-1</sup> methoxyaminhydrochloride in pyridine) followed by 30 min shaking at 37°C in 80 µl  
265 BSTFA mixture (70 µl N,O-bis(trimethylsilyl)trifluoroacetamide + 10 µl alkane mix). The  
266 derivatized metabolites were subjected to GC-MS analysis (Agilent technologies 7890, USA)  
267 coupled with mass spectrometry. Measurement from an injection volume of 1 µl was taken in  
268 split-less mode in DB-5 column (30 m × 0.25 mm, 0.25 µm film thickness, Agilent) using

269 helium as carrier gas. Metabolites were separated as described by Wagner et al. (2013).  
270 Qualitative analysis of chromatograms was performed in MassHunter Qualitative analysis  
271 Sp1 workstation (Agilent, USA). Identification and annotation of each compound was  
272 supervised manually using AMDIS software and NIST08 database  
273 (<http://www.nist.gov/srd/mslist.html>). Data were normalized to sample weight and internal  
274 control (sorbitol). Statistical analysis was performed as described earlier (Quanbeck et al.,  
275 2012). Log<sub>2</sub> ratio of metabolite abundances in -Fe was plotted against +Fe. Delta method  
276 approximation was used to calculate standard errors (se) of log-ratio,  $se \log\text{-ratio} = 1/\ln$   
277  $2\sqrt{[(SE_T / T)^2 + (SE_C / C)^2]}$ , where  $SE_T$  and  $SE_C$  are standard errors of average -Fe and +Fe  
278 metabolite abundances.

279

### 280 *Measurement of glutathione-S-transferase (GST) activity and iron mobilization assay for PS* 281 *estimation*

282 Activity measurement of GST was performed in the wheat roots subjected to -Fe for 10, 15  
283 and 20 days of treatment along with the control plants (no stress) as mentioned in plant  
284 materials. The estimation was done using Glutathione-S-transferases assay kit (Sigma, USA).  
285 Briefly, 100 mg of tissue was used for total protein extraction. Equal amount of total protein  
286 (25 µg) was used as a source of enzyme and 1-Chloro-2,4-dinitrobenzene (DNB) was used as  
287 a substrate. The resulting GS-DNB conjugate was measured at 340 nm wavelength during the  
288 time course of the reaction. The direct increase in absorption was measured and GST activity  
289 was calculated as described in the manufacturer instruction kit.

290 For PS release, iron mobilization assay was performed as described earlier (Takagi et  
291 al., 1976). Briefly, 10 seedlings (each for -Fe and +Fe for 10 days treatment) were used for  
292 the experiment. After treatment the seedlings were subjected to PS release after 2 hours of  
293 onset of light period in aerobic condition for 3 hrs in 20 ml deionised water with 10 mgL<sup>-1</sup>  
294 Micropur (Katadyn, Switzerland). Next, 2 ml of freshly precipitated solution of Fe(OH)<sub>3</sub> and  
295 0.5 ml of 0.5 M Na acetate buffer (pH 5.6) was added to 8 ml of the collection solution. The  
296 solution was shaken for 2 hrs and subsequently was filtered (Whatman #1) into 0.2 ml of  
297 6NHCl. Ferric iron was reduced by addition of 0.5 ml of 8% hydroxylamine-hydrochloride  
298 and heating to 60 °C for 20 min. The total concentration of ferrous iron was calculated by  
299 measuring absorbance at 562 nm after adding 0.2 ml of 0.25% ferrozine and 1 ml of 2 M Na-  
300 acetate buffer (pH 4.7).

301

302 *Elemental analysis using inductive coupled plasma-mass spectroscopy and nitrate estimation*  
303 Elemental analysis in roots and shoots was performed using Inductive Coupled Plasma-MS  
304 (ICP-MS). Metal analysis was performed as described earlier (Bhati et al., 2016; Aggarwal,  
305 2018). Briefly, the samples were ground to fine powder and subsequently subjected to the  
306 microwave-digested with HNO<sub>3</sub> as described earlier (SuraPure<sup>TM</sup>, Merck). Respective metal  
307 standards were also prepared for analysis. Three independent replicates from the experiments  
308 were used for metal analysis.

309 Nitrate content in wheat roots was measured according to method described  
310 previously (Cataldo et al., 1975). Briefly, 1 g of fresh tissue was homogenized in 6 ml of  
311 deionised water and centrifuged at 30,000g for 15 min. The 100 µl of supernatant was added  
312 to 400 µl of salicylic acid (w/v dissolved in conc. H<sub>2</sub>SO<sub>4</sub>). After mixing the reaction was kept  
313 at room temperature for 20 min. 2N NaOH (9.5ml) was then added slowly to raise the pH  
314 above 12. The samples were allowed to cool and readings were taken at 410nm in  
315 spectrophotometer.

316

## 317 **Results**

318

### 319 *Fe starvation affects wheat growth capacity and nutrient uptake*

320 Fe starvation is known to affect plant growth capacity. In order to determine the effect of Fe  
321 starvation, one-week old wheat seedlings, grown on complete medium (presence of Fe) were  
322 transferred to Fe starvation media for additional days. After 20 days of starvation (DAS) the  
323 wheat seedlings started showing strong phenotypic symptoms including visible chlorosis and  
324 therefore detailed study was performed for this specific time point. In response to Fe  
325 starvation, plants showed decrease in the shoot biomass with an enhanced chlorosis  
326 phenotype and shortening of the root system compared to control wheat seedlings (Fig. 1A  
327 and B). Roots of Fe-starved wheat seedlings showed decrease in number of lateral roots and  
328 significant reduction in the primary root length in comparison to control plants (Fig. 1C and  
329 D). Earlier studies have suggested that changes in the root system and Fe supply not only  
330 affect the Fe accumulation capacity but also impacts the uptake of other nutrients such as Zn,  
331 Cd etc. (Sperotto et al., 2012; Shukla et al., 2017). Therefore, effect of Fe starvation stress on  
332 the uptake of Zn, Mn, Cu, and Mg in wheat undergoing Fe stress was studied (Table 1). Out  
333 data indicated increased uptake of nutrient elements such as Zn, Mn, Cu, and Mg in roots but  
334 accumulation in shoots was either unaltered or decreased. This further support the importance

335 to study root response to Fe starvation to gain insight on the molecular mechanism evolved  
336 by wheat to cope with nutritional stress.

337

338 *Differential expression analysis, homoeolog (A, B and D) induction and expression bias*  
339 *during –Fe response*

340 The effect of Fe starvation on the wheat root transcriptome has not been investigated till date.  
341 To perform this study, RNAseq technology was used to identify the changes in the transcripts  
342 of wheat roots, where plants were grown in presence or absence of optimal Fe (20 DAS). Our  
343 analysis resulted in 87 million quality filtered reads, with an average of nearly 22 million  
344 reads from each sample (more than 87% reads had a quality score greater than Q30). Filtered  
345 reads from the four libraries had a mapping rate ranging from 81.7% to 85.4% when mapped  
346 against release-37 of the wheat genome using TopHat (Supplementary Table S2). As quality  
347 check, a strong correlation within the two biological replicates from each condition was  
348 observed, while a clear variation was seen between the two conditions (Fig. 2A). We  
349 thereafter analysed the expression values as FPKMs (Fragment Per Kilobase of transcript per  
350 Million mapped reads), calculated by using Cufflinks software. Differentially expressed  
351 genes (DEGs) were then identified by calculating logFC (log<sub>2</sub> fold change) and performing  
352 statistical tests between FPKM values from control and stressed samples using CuffDiff.  
353 50610 genes with an FPKM of greater than or equal to 1 in at least one of the two conditions  
354 were considered to be “expressed transcripts”. In all, 7221 genes had logFC > 0 and 8010 had  
355 logFC < 0 (Fig. 2B). On setting up a criterion of logFC of more than 1 for up-regulated genes,  
356 and that of less than -1 for down-regulated genes and an FDR < 0.05, a total of 3478 genes  
357 were highly expressed, whereas, 2376 were down-regulated under –Fe condition in wheat  
358 roots (Fig. 2C). Interestingly, 45 genes were also induced exclusively during starvation  
359 condition when compared to the control samples (Fig. 2C, Supplementary Table S3).

360 Our data allowed us to analyse the chromosomal distribution of the DEGs under the –  
361 Fe condition. While all chromosomes contributed the DEGs, the highest number of genes was  
362 mapped on chromosome 2 of the wheat genome (Fig. 3A). Equal representation of transcripts  
363 was observed for the chromosome 7 and 5. The remaining chromosomes, 1, 3, 4 and 6  
364 showed 15, 13, 12 and 10% distribution of DEGs, respectively. In polyploidy crops like  
365 wheat, homoeolog induction bias could impact plant response to various stresses (Liu et al.,  
366 2015; Powell et al., 2017). To determine the extent of induction bias (from A, B and D sub-  
367 genomes) in wheat during Fe starvation, homoeolog specific expression analysis was  
368 performed. Starting from a list of 8473 gene triplets present/expressed selected as ‘accepted

369 triplets' (Supplementary Table S4), most of homoeolog triplets (8349) showed no significant  
370 biasness in expression ( $A = B = D$ ). Out of these, 8321 triplets appeared to be unaffected by –  
371 Fe stress, while 22 and 6 homoeologous triplets were up- and down-regulated respectively.  
372 Homoeolog expression bias was observed in 124 homoeolog triplets. Eighty-seven triplets  
373 had only one of the homoeologs differentially expressed (up- or down-regulated). Sub-  
374 genome specific contribution towards this biasness within triplets is depicted in left panel of  
375 Fig. 3B. These include forty-seven in the category '1UP' with  $A > B = D$ ,  $B > A = D$  and  $D >$   
376  $A = B$ , 40 in category named '1DOWN' having  $A < B = D$ ,  $B < A = D$  or  $D < A = B$ . Table 2  
377 provides the list of genes with significant induction predominance occurring from the A and  
378 B genomes in response to Fe starvation . Few of the prominent transcripts exclusively  
379 induced by these two genomes include transcripts related to MYB TFs, metal transporters,  
380 zinc transporters, RINGH-H2 type proteins, genes belonging to major facilitator superfamily  
381 proteins etc. Additionally, 37 triplets had two of the homoeologs differentially expressed  
382 while the third showed normal expression even under Fe stress (Fig. 3B; right panel). '2UP'  
383 category includes  $AB > D$ ,  $AD > B$  and  $BD > A$  while '2DOWN' includes  $AB < D$ ,  $AD < B$   
384 and  $BD < A$  (Fig. 3B). This suggests that during Fe starvation, the additive homoeolog  
385 contribution from either A or B sub-genome was the highest.

386 For polyploid genomes such as wheat, the interaction of its sub-genomes is known to  
387 affect the final phenotype or contribute towards trait development (Borrill et al., 2015). To  
388 check the homoeolog/sub-genome expression biasness under –Fe condition, effect on the  
389 expression of transcripts from the genomes was performed by comparing the relative  
390 normalised expression for each homoeolog within a triad. This resulted seven combinations  
391 including one balanced category and six homoeolog specific dominance or suppression  
392 categories. Our analysis reflected that most of the triads were falling under the balanced  
393 category (Table 3 and Fig.3C). This category was represented by 77% and 77.89% of the  
394 total triads for control and Fe starvation condition. Triads with unbalanced expression varied  
395 in the range of 0.94 to 7.09 for all the 6 sub-categories across the two conditions (Table 3 and  
396 Fig.3C). Our analysis revealed that maximum genome specific expression biasness was  
397 observed for A and B on both the conditions. Interestingly, D genome was least suppressed  
398 with a representation of 5.15% of the total triads taken in consideration in control when  
399 compared to 4.93% in Fe starvation. 89% triads showed conserved balanced/unbalanced  
400 contribution across both conditions. Overall, a higher relative abundance of D genome  
401 (Control: 33.94%; –Fe: 33.95%) was noted as compared to the A (Control 33.06%; –Fe:  
402 33.00%) and B (Control: 33.04%; –Fe: 33.95%) genomes.

403

404 *Identification of DEGs pinpoints the prolific expression of genes involved in Strategy-II mode*  
405 *of Fe uptake*

406

407 To identify the transcripts differentially expressed in roots in response to Fe starvation, top 50  
408 genes either up-regulated or down-regulated were shortlisted (Fig. 4). Expression of most of  
409 the highly up-regulated transcripts ranged from 12 to 4.8 log<sub>2</sub> fold change (Supplementary  
410 Table S3) indicating their higher fold accumulation under Fe starvation compared to the  
411 control conditions. As observed in the top 50 upregulated genes, the predominance of  
412 pathway genes encoding the components for Strategy-II mode Fe uptake was observed across  
413 all the 3478 upregulated genes. Categorically, these highly induced genes are known to be  
414 involved during Strategy-II mode of iron uptake, including the sub-family of nicotinamine  
415 synthase (NAS) and deoxymugineic acids (DMA) biosynthesis genes (Fig. 4, left panel).  
416 Other important genes include genes belonging to the Major Facilitator Superfamily  
417 including an ABC transporter, zinc-induced facilitator like transporters (ZIFL), sulphate  
418 transporters. Therefore, under Fe starvation, the DMAS biosynthesis genes were highly  
419 induced. Similarly, YSL genes were significantly induced under Fe starvation condition. All  
420 the homoeologs of *TaYSL9* and *TaYSL1A* showed especially high expression under starvation  
421 condition (Supplementary Table S5). On the similar lines, genes encoding for NRAMP also  
422 showed high transcript abundance in roots subjected to Fe starvation (Supplementary Table  
423 S5). The validation of the expression of few Strategy-II uptake genes was also done by  
424 quantitative real time-PCR (qRT-PCR). Our results for qRT-PCR validate our inference from  
425 the RNAseq analysis. Almost all of the Strategy-II genes tested for their expression showed a  
426 very high fold expression in Fe starved roots as compared to the control (Supplementary Fig.  
427 S1). Highest expression was obtained for ZIFL4, DMAS1, NAAT1, NAS1 those are the  
428 prime components for Strategy-II mediated uptake. Other transcripts encoding for thaumatin  
429 like proteins etc. were also induced under Fe limiting condition.

430

431 Transcripts of genes involved in the Strategy-I mode of Fe uptake were also analysed  
432 (Supplementary Table S6). An important component of Strategy-I pathway that includes H<sup>+</sup>-  
433 ATPase (AHA) subfamily genes was not differentially expressed under Fe limiting condition  
434 (Supplementary Table S6). This was in agreement with the qRT-PCR analysis where, either  
435 no change or down-regulation of AHA genes was observed (Supplementary Fig. S1) in wheat  
436 roots. Metallo-reductases are important components of Strategy-I represented by ferric-  
chelate reductase (FRO). Most of the transcripts encoding for wheat FROs do not show

437 significant changes in starved roots as compared to control except for one transcript.  
438 Interestingly, iron regulated transporters (IRT;  
439 TRIAE\_CS42\_7DS\_TGACv1\_622068\_AA2032200;  
440 TRIAE\_CS42\_4AL\_TGACv1\_289466\_AA0971640) were significantly expressed in Fe  
441 starved wheat roots, suggesting their involvement in wheat under metal stress. The high  
442 expression of *TaIRT1* was also confirmed by qRT-PCR (Supplementary Fig. S1). This suggest  
443 that IRT function might be conserved among the plant species.

444 In addition to this, forty-five genes showed exclusive transcript abundance under Fe  
445 starvation (Supplementary Table S3). No transcript for any of these genes was detected in the  
446 control root samples, suggesting their high specificity for Fe response. Some of the  
447 transcripts responding to Fe starvation encode for metallothionine, metal transporters,  
448 vacuolar iron transporters (VIT1) and nicotianamine synthase 2 (NAS2). This suggests that in  
449 wheat few components involved in Fe uptake could actually respond exclusive to Fe  
450 starvation. The fold expression levels of genes those were highly down-regulated ranged  
451 from -7.1 to -2.85-fold at the level of log<sub>2</sub> scale (Supplementary Table S3). Interestingly,  
452 multiple genes encoding for nitrate transporters were highly down-regulated under Fe  
453 limiting condition (Fig. 4, right panel). Two genes encoding for cytochrome-P450 also  
454 showed down-regulation. Among the others, genes encoding for Histone deacetylase,  
455 peptidases A1 containing domain protein, cinnamyl alcohol dehydrogenase, dirigent protein  
456 show significant down-regulation.

457

#### 458 *Functional enrichment network of Fe starvation related genes*

459 Gene ontology annotations and classification of DEGs was performed to get the overview of  
460 processes those are representation of cellular, molecular and biological functions. Analysis  
461 was further extended to cluster analysis using Cytoscape plugins, BINGO and Enrichment  
462 Map (Maere et al., 2005; Merico et al., 2010). A total of 5854 DEGs were found to be  
463 differentially-expressed in response to Fe starvation; significant GO categories were assigned  
464 to all DEGs. The DEGs annotated for GO terms were visualized using WEGO tool (Fig. 5A,  
465 Supplementary Table S7). Most enriched GO terms in the “cellular component” category  
466 were membrane and intracellular organelle. Other overrepresented terms included catalytic  
467 activity and ion as well as organic compound binding for the “molecular function” category,  
468 while metabolic processes related to nitrogen as well as other cellular processes were  
469 observed for “biological process” category (Fig. 5A). Overall, catalytic activity and binding  
470 activities were most significantly enriched GO terms in -Fe condition (Fig. 5B). Further

471 mapping of upregulated genes to databases such as, Kyoto encyclopedia of genes and  
472 genomes (KEGG) pathway (Xie et al., 2011) and MapMan (Thimm et al., 2004) revealed  
473 enrichment related to phenyl-propanoid biosynthesis, amino acid biosynthesis and carbon  
474 metabolism, and glutathione metabolism (Fig. 5C and Supplementary Fig. S2). The role of  
475 glutathione in response to Fe starvation is intriguing and deserves further investigations.

476 GO category “integral to membrane” was found to be associated with pathways  
477 clustered into “metal ion and trans-membrane transport” and “photosynthesis” related GO  
478 categories (Fig. 6A). Clustered pathways involved in “response to nutrient levels” and  
479 “Sulphur amino acid metabolism” was also enriched (Fig. 6A). A few other up-regulated  
480 clustered pathway genes involved fall into the category “response to phosphate starvation”. In  
481 the enriched network of down-regulated DEGs, genes involved in iron and other metal  
482 homeostasis were associated with two different clusters, mainly included genes related to  
483 lipid, ketone and carboxylic metabolism, in addition to those involved in nitric acid and  
484 salicylic acid response (Fig. 6B). A second cluster contains transcripts related to purine and  
485 adenine nucleotide binding and pyrophosphatase activity. Thus, whole set of significant up-  
486 regulated and down-regulated DEGs were clustered in distinct cellular processes suggesting  
487 differential transcriptional response under Fe starvation.

488

#### 489 *Identification of transcriptional regulatory genes during Fe starvation*

490 To address an important question on how the –Fe signal is connected to the transcriptional  
491 machinery in wheat, genes encoding TFs were identified. Earlier the TFs involved in the  
492 response to Fe starvation were identified in the model plant Arabidopsis and rice including  
493 POPEYE (PYE), basic helix-loop helix (bHLH), ethylene insensitive-3 (EIN3), EIN3-like1  
494 (EIL1) (Long et al., 2010, Mai et al., 2016, Bauer et al., 2011, Ivanov et al., 2012; Ogo et al.,  
495 2011; Bashir et al., 2014). Consistently, our transcriptome analysis showed that all  
496 homoeologs for PYE encoding a bHLH transcription factor and BRUTUS-like (BTS) known  
497 to encode a putative hemerythrin E3 ligase protein in Arabidopsis and rice were highly  
498 expressed in wheat roots under Fe starvation (Supplementary Table S8). Analysis of these  
499 category of genes led to identification of 41 significantly up-regulated TF family members  
500 ( $>\log_2FC$ ) (Supplementary Table S8). The TF family members belong to categories like  
501 APETALA2 ethylene-responsive element binding proteins (AP2/EREBP), WRKY, C2H2,  
502 Zinc finger proteins (including C3HC4), NAM, bHLH hemerythrin and U-box (Fig. 7A). Out  
503 of these, transcripts encoding for AP2/EREBP followed by WRKY and bHLH were the most  
504 abundant in wheat. Genes encoding for AP2-EREBP, WRKY and C2H2 type of TFs also

505 showed high predominance (Supplementary Table S8 and Supplementary Fig. S3). However,  
506 genes encoding for TFs such as MADS, PHD and homeobox (HB) domain containing  
507 proteins were highly represented in the list of down-regulated transcripts. Finally, to ascertain  
508 regulatory functions under iron starvation, enrichment mapping was performed for the  
509 significantly expressed DEGs those were classified into transcriptional factors. Interestingly,  
510 genes involved in regulation of gene expression were clustered with primary and nucleotide  
511 metabolism related genes in both positive and negative correlation. This functional cluster  
512 was in positive correlation with TFs involved in gene ontology (GO) categories such as  
513 “vacuolar transport” and “DNA topoisomerase III activity”. However, two separate clusters  
514 “cellular response to auxin stimulus and signalling” and “cell-fate specification” were in  
515 negative correlation with “regulation of gene expression” and “primary and nucleotide  
516 metabolism” (Fig. 7B). This suggested an important regulatory role of TFs involved in auxin  
517 signalling and cell-fate specification in Fe starvation response control, thereby modulating  
518 the network of Fe homeostasis.

519

#### 520 *Glutathione-S-transferases are involved in the response to Fe starvation in wheat*

521 Glutathione mediated conjugation of multiple metabolites plays important role during the  
522 metal stress (Zhang et al., 2013). Our transcriptome data revealed the enhanced expression of  
523 multiple glutathione-S-transferases (GST) in Fe-starved wheat root as compared to control  
524 (Supplementary Table S9). To correlate the expression response with its enzymatic activity,  
525 temporal response of GST was measured in wheat roots under –Fe conditions. Using the GST  
526 functional assay, the activity was determined in wheat roots of plants grown for 10, 15 and 20  
527 days under Fe starvation. Our activity assays showed significant increase in the GST activity  
528 under –Fe condition, which peaked at 10 and 20 days after the beginning of Fe starvation  
529 compared to control plants (Fig. 8A). Therefore, our experiments validate the increased GST  
530 transcript abundance with enhanced glutathione activity. These results indicate an important  
531 role of glutathione in response to Fe starvation in wheat roots.

532

#### 533 *Fe starvation causes an accumulation of organic acids and polyhydroxy acids in wheat*

534 To obtain a comparative insight of the metabolite profile of wheat roots of plants grown in  
535 absence or presence of Fe; GC-MS profiling analysis was performed. Metabolites were  
536 extracted from the roots of three replicate pools of plants each containing eight seedlings.  
537 Qualitative processing of each chromatogram for peak area and identification was performed  
538 in MassHunter version B.05.00 software coupled with NIST11 compound library. The

539 compound annotation was determined by comparing individual resolved peaks to library  
540 searches based on mass spectra and compounds chromatographic retention indices.  
541 Interestingly, analysis resulted in the identification of 54 metabolites and further 39 annotated  
542 metabolites were analysed for their response ratio (Supplementary Table S10). To compare  
543 the change under Fe-starvation, metabolite abundances (-Fe roots/control roots) were  
544 calculated and expressed in Log2 fold change values. Fe-starvation significantly affected  
545 accumulation of 22 metabolites that includes organic acids, polyhydroxy acids, amino acids  
546 and some of the sugars, fatty acids and phosphates (Fig. 8B). Amongst treatment-specific  
547 changes, few organic acids such as fumaric acid, acetic acid and malonic acid showed higher  
548 level of accumulation in Fe starved roots as compared to the control. In contrast, citric acid,  
549 malic acid, valeric acid and aconitic acid were significantly lowered in Fe starved roots when  
550 compared to control samples. In Fe-starved roots, the accumulation of amino acids mainly, L-  
551 Valine showed significant increase while hydroxyl butyric acid and pyroglutamic acid was  
552 lowered in comparison with control roots. Polyhydroxy acids like gluconic acid and glyceric  
553 acid were also significantly high in Fe starved roots, whereas level of hexonic acid and  
554 arabinic acid was found to be low. Taken together, our results showed that during Fe  
555 starvation wheat roots undergo reprogramming for metabolic changes to maintain the Fe-flux.

556

## 557 **Discussion**

558

559 How plants maintain nutrient homeostasis is a fascinating question in plant biology. In this  
560 direction, *A. thaliana*, with its fully sequenced small genome has provided some basic  
561 information. Developing our knowledge on nutrient homeostasis in crops, especially those  
562 having complex genomes, including hexaploid wheat is more challenging. Recently, the  
563 release of genome sequence, generation of transcriptome data and the advancement of  
564 different functional tools have provided much needed impetus in this direction (Borrill et al.,  
565 2015). The current study was undertaken to gain insight into the response of hexaploid wheat  
566 exposed to Fe starvation that is known to severely affect crop production. In this study,  
567 transcriptome of wheat (cultivar C306) in response to Fe starvation was generated. Our  
568 analysis revealed that; (a) wheat utilizes primarily Strategy-II mode of Fe uptake, (b)  
569 accumulates transcripts encoding for methionine-salvage pathway coupled with enhanced  
570 GST activity and (c) accumulates specific metabolites including fumarate, acetate, malonate  
571 and xylofuranose, to efficiently mobilize soil Fe. Interestingly, our systematic analysis of  
572 expression data revealed that transcripts show an induction biasness for A and B genomes of

573 wheat in response to –Fe condition. Overall, this work provides the first comprehensive  
574 insight at the molecular level for wheat roots during Fe-deficiency.

575 Wheat plants subjected to Fe starvation show physiological defects such as a decrease  
576 in the root growth. This phenotype was consistent with the previous report showing negative  
577 impact on the root growth of wheat seedlings under Fe stress (Garnica et al., 2018). Our  
578 analysis also suggested down-regulation of few nitrate transporters for the time point studied.  
579 Homology searches indicated the identified nitrate transporters in wheat as  
580 *TaNRT2.2* and *TaNRT2.3* (Buchner and Hawkesford, 2014). These observations suggest that  
581 Fe starvation represses nitrate transporters, which in turn leads to lower accumulation of  
582 nitrate levels in the roots (Supplementary Fig. S4). Although impact of Fe starvation on the  
583 nitrate metabolism has not been studied in detail, yet similar decrease in nitrate levels were  
584 also observed in cucumber shoots subjected to –Fe condition (Borlotti et al., 2012). This  
585 observation further reinforces the existence of an interaction between macro and  
586 micronutrients in plants, which has recently gained attention (Rouached and Rhee, 2017;  
587 Bouain et al., 2019).

588 Due to the low availability of micronutrients in soil, plants are equipped in recruiting  
589 components that could participate in the two major strategies for Fe uptake (Kobayashi and  
590 Nishizawa, 2012). Cereals such as maize and rice predominantly utilize Strategy-II mode of  
591 uptake, unlike Arabidopsis, that employs Strategy-I mode of Fe uptake (Li et al., 2014; Zanin  
592 et al., 2017; Hell and Stephan, 2003). Nevertheless, a comprehensive study to identify the  
593 molecular players involved during Fe limiting conditions in wheat is lacking. Our RNAseq  
594 based analysis, strongly suggested an increase in the transcript abundance of genes for  
595 Strategy-II mode of Fe uptake. With the exception of conserved genes like *IRT1* (iron  
596 regulated transporter), prime genes for Strategy-I uptake mechanism like *FRO* (Ferric chelate  
597 reductase) and proton *H-ATPase* (AHA-like) were also present during starved condition but  
598 at very low abundance and no *FRO* activity has been reported for cereals. During this study,  
599 wheat root subjected to Fe starvation also does not show any *FRO* activity (data not shown).  
600 Therefore, our results reveal that wheat utilize Strategy-II mediated uptake of Fe and induces  
601 *IRT* genes that might be conserved for their function across the plant kingdom.

602 The series of events during Strategy-II uptake mechanism used by Gramineae  
603 involves secretion of PS that facilitate conjugation of Fe to form Fe-complexes. These Fe-PS  
604 complexes are imported in roots for remobilization to the different developing organs. As  
605 represented in Figure 9, the transport of these Fe-complexes occurs via membrane  
606 transporters via ZIFL genes encoding for TOM proteins (Nozoye et al., 2011; Nozoye et al.,

607 2015). Multiple wheat ZIFL show high transcript accumulation and are closest homolog of  
608 OsTOM1 from rice, thereby speculating its role in Fe acquisition. Utilizing gain- and loss of  
609 function approaches OsTOM1 has been demonstrated to be a DMA effluxer for its role in  
610 enhancing mobilization and thereby improving Fe uptake (Nozoye et al., 2011). Altogether,  
611 based upon the high similarity and response under Fe starvation, it is tempting to propose  
612 wheat ZIFL (ZIFL4) as a functional transporter of DMA. Although, other *ZIFLs* were also  
613 significantly expressed but functional wheat transporter for DMA needs to be deciphered. PS  
614 secretion was also observed during our analysis for the roots of C306 exposed to Fe  
615 starvation. In this study a high PS release of  $\sim 40\text{-}45 \text{ nmol g}^{-1} \text{ root biomass (3 hrs)}^{-1}$  was  
616 observed, reinforcing our RNAseq data that DMA biosynthesis genes and its transporters  
617 were highly upregulated. Control plants show accumulation of  $\sim 1\text{-}2 \text{ nmol g}^{-1}$  suggesting that  
618 wheat releases a basal level of PS to maintain the constant flux of Fe in roots. Upon careful  
619 analysis of the RNAseq data, it was observed that multiple such efflux transporters are  
620 represented in the list that are highly abundant under Fe starvation. During our study, we  
621 identified *TaDMAS1* encoding for deoxymugineic acid synthase that was highly responsive  
622 for Fe starvation (Supplementary TableS5). Earlier, *TaDMAS1* was reported as a gene that  
623 was broadly expressed across the tissue and was regulated during Fe-starved condition. These  
624 observations support the notion that *TaDMAS1* has potential to enhance the seed iron storage  
625 capacity (Beasley et al., 2017). During our study, GO term enrichment was also observed for  
626 DMA biosynthesis pathway, transmembrane transporters and cellular response that reinforce  
627 importance of these functional categories. Surprisingly, genes pertaining to photosynthesis  
628 were also observed. This anomaly could be explained by the presence of active photosystem  
629 in the basal roots of our collected wheat tissue, similar to that observed in Arabidopsis due to  
630 the changes in the auxin/cytokinin ratio (Kobayashi et al., 2012). Secondly, during this study  
631 the wheat roots under Fe starvation show significant accumulation of two Golden-2 like  
632 (GLK) TF's ( $\sim \log_{2}\text{FC } 1.54 \text{ and } 1.55$ ; Supplementary Table S3). GLK's are known to improve  
633 phototrophic performance of roots and thereby enhancing root photosynthesis (Kobayashi et  
634 al., 2013). These reasons may account for the enhanced accumulation of transcripts related to  
635 photosynthesis along with other metabolic related genes.

636 Wheat is a hexaploid crop with three genomes and therefore studying the homoeolog  
637 induction and expression bias could provide an insight on the regulation of the transcript  
638 under a given biotic and abiotic stress. Therefore, we subjected our RNAseq data to these  
639 analyses. In depth analysis confirms the minimal suppression for the expression bias for the  
640 D-genome derived transcripts as compared to A or B. These observations support the

641 previous analysis wherein, suppression of D genome was significantly less frequent in  
642 multiple tissue (Ramirez-Gonzalez et al., 2018). Earlier, homoeolog expression was also  
643 studied for wheat under infection with *Fusarium pseudograminearum*, wherein the  
644 expression bias was observed for B and D subgenomes (Powell, et al., 2017). Utilizing  
645 RNAseq data, changes in the pattern of the homoeologous gene expression were also  
646 reported in bread wheat (Leach et al., 2014). Therefore, such studies are important to pin-  
647 point actively expressed/induced homoeologs that could be targets for genetic improvement.  
648 However, the genome biasness and its association with the secretion of siderophores,  
649 genotypic variability in a complex wheat genome has yet to be investigated. Previous studies  
650 have shown that the phytosiderophores release mechanism in wheat is effective when the  
651 three genomes A, B and D contribute synergistically to induce its biosynthesis and release. In  
652 general, genome induction biasness for A and B genome was observed for the hexaploid-  
653 wheat under Fe stress (Fig. 3B). Interestingly, these genomes were also suggested to be  
654 important during starvation of other micronutrients like Zn (Tolay et. al., 2001). These  
655 observations provide clue for the importance of A and B genomes during micronutrient  
656 starvation in hexaploid wheat when compared to their progenitor. The PS release intensity is  
657 also dependent on complementary action of the genotypic ploidy with the following the  
658 pattern, *T. aestivum* (BBAADD) > *T. dicoccum* (BBAA) > *T. monococcum* (AA) > *Ae.*  
659 *tauschii* (DD) (Ma et al., 1999; Tolay et al., 2001).

660 Multiple genes for the salvage pathway were highly up-regulated including *NAS1*,  
661 *NAS2* and *NAAT1* (Supplementary Table S3 and Supplementary Table S5). The contribution  
662 of these transcripts arises from different genomes suggesting that all the genomes of wheat  
663 are capable of responding to the starvation condition. Based on our RNAseq analysis it is  
664 likely that the gene encoding for *TaYSIA* and *TaYSL9* could be the putative transporter for  
665 Fe-siderophore complex. Previous, studies have indicated the high response of *TaYSIA* under  
666 Fe starvation in roots and shoots (Kumar et al., 2019). Out of the closest orthologs of wheat-  
667 *YSIA*, *HvYSIA* and *ZmYSIA*, *HvYSIA* has been shown to be involved in specific transport of  
668 Fe whereas, *ZmYS1* was reported to have broad substrate specificity (Schaaf et al., 2004).  
669 Our RNAseq data also revealed a conserved function of genes from monocots and dicots  
670 during the Fe regulation and known important Fe regulators such as *PYE* and *BRUTUS* also  
671 showed differential expression in wheat roots (Ivanov et al., 2012). Same for TFs spanning  
672 multiple gene families such as *MYB* (Rubio et al., 2001), *bHLH* (Colangelo et al., 2004;  
673 Jakoby et al., 2004; Ogo et al., 2007), *C2H2*, *NAC*, *AP2-ERB* (Kim et al., 2012), and *WRKY*  
674 (Devaiah et al., 2007) were characterized in Arabidopsis and rice for their involvement in

675 nutrient uptake which were found to be highly represented in root of Fe-starved wheat.  
676 Similarly, hemerythrin motif-containing protein were also overexpressed in our study. As in  
677 case of other graminaceous plants like rice, hemerythrin domain containing proteins  
678 including OsHRZ homolog for Arabidopsis BRUTUS was also differentially perturbed in –  
679 Fe (Kobayashi et al., 2014). Overall, based on the information obtained from our studies  
680 future research focus should be able to gain better insights of the molecular functions of these  
681 genes using tilling population in wheat and/or a heterologous system.

682 Changes in metabolite content in response to Fe-deficiency can lead the plant to  
683 undergo adaptive processes to maintain iron homeostasis (Schmidt et al., 2014). A schematic  
684 representation of data provides a comprehensive summary of the metabolic and  
685 transcriptional changes that occur during Fe starvation in wheat roots (Fig. 9). The  
686 mobilization and transport of Fe inside the plant tissue depends on its speciation and  
687 complexation form. Depending on the tissue, Fe could form a complex with multiple  
688 metabolites such as nicotianamine, malate, citrate that facilitates the transport through the  
689 phloem and xylem (Grillet et al., 2014; Palmer et al., 2013). Our analysis for the metabolome  
690 of roots suggested predominance of additional organic compounds such as fumarate, acetate,  
691 glycerate etc. thereby, suggesting that they could be also involved in Fe-complexation to  
692 assist in long distance transport and remobilization to different tissues (Fig. 9). These  
693 metabolites are reported for their ability to complex with Fe(III) state during the transport in  
694 the xylem vessels as detected during the X-ray absorption near-edge structure spectroscopy  
695 based studies (Terzano, et al., 2013). Similarly, the accumulation of glycerate could be  
696 responsible for added thrust towards glycerate-serine pathway during Fe starvation (Figure  
697 9). Glycerate-serine pathway are important to generate methionine and precursor (S-adenosyl  
698 methionine) of DMA biosynthesis. Consistent with the metabolome data, the transcripts  
699 encoding these proteins were highly upregulated in our study as presented by the bins (Figure  
700 9). Members of ABC-B transporters were also reported to participate in oxidative stress that  
701 was linked with metal stress including Fe starvation (Kispal et al., 1997; Schaedler et al.,  
702 2014). During our analysis we have identified a TAP type, ABCB subfamily transporter  
703 referred to as *TaABCB25* that was highly upregulated during Fe starvation (Fig. 4). The  
704 closest ortholog for wheat ABCB25 transporters were identified in rice (*OsABCB25*) and  
705 Arabidopsis (*AtABCB27*) (Supplementary Fig. S5A). The temporal-induction of *TaABCB25*  
706 was also re-confirmed in roots subjected to Fe starvation (Supplementary Fig. S5B).  
707 *Arabidopsis thaliana* ABCB27 was shown to have the ability to transport glutathione  
708 conjugate metabolite precursors for the Fe-S cluster assembly (Schaedler et al., 2014). Based

709 on the presence of domain structure these ABCB transporters from rice, *Arabidopsis* and  
710 wheat qualify as half-size transporter (Supplementary Fig. S5C). In graminaceous species,  
711 glutathione related activity was observed to be highly upregulated under Fe deficient  
712 condition supporting our observation in the current study (Bashir et al., 2007). Enhanced  
713 GST activity in wheat under Fe starvation and the abundance of *TaABCB25* in roots, warrants  
714 further study of this gene for its role in mobilizing micronutrient uptake. Glutathione and  
715 GST plays an essential role during Fe starvation related responses in *Arabidopsis* and  
716 also quench reactive molecules to protect the cell from oxidative damage and prevent  
717 chlorophyll loss (Ramirez et al., 2013; Shanmugam et al., 2015; Kumar and Trivedi, 2018).  
718 Our analysis also suggests that high transcript and enzyme activity of GST could be linked  
719 with the primary metabolism since it accumulates fumarate (Fig. 9). In *Arabidopsis*, it has  
720 been shown that GST catalyses Glutathione-dependent isomerization of maleyl-acetoacetate  
721 into fumaryl-acetoacetate eventually leading to accumulation of fumarate and acetoacetate  
722 (Dixon et al., 2002). Additionally, GST is also linked with the conjugation of the reduced  
723 glutathione (GSH) forms to various substrate to make it water soluble. The sulphur derived  
724 metabolite and glutathione are well known to be involved in biosynthesis methionine, a well-  
725 known precursor for DMA biosynthesis (Forieri et al., 2013). Altogether, this supports the  
726 notion that in wheat role of glutathione is important during Fe starvation and ABC  
727 transporters might play a significant role in mobilization of metabolite/organic acid or  
728 specific siderophores.

729 In conclusion, in this study, the core components for Fe starvation response in  
730 hexaploid wheat have been identified so as to provide a better understanding of the molecular  
731 events that participate during Fe starvation in wheat roots. In particular, we provide line of  
732 evidence for the role of GST in the response to -Fe in roots. Complementary approaches,  
733 analytical and transcriptome analysis reinforce the importance of primary metabolism for  
734 reprogramming organic acids and amino acids thereby leading to the Fe homeostasis in  
735 wheat. The information here not only help to design strategies to improve plant response to  
736 Fe starvation in wheat, but will also foster Fe uptake and accumulation studies, which are  
737 required to boost productivity and grain nutritional quality through Fe biofortification  
738 programs.

739

#### 740 **Acknowledgement**

741 Authors thank Executive Director, NABI for facilities and support. This research was funded  
742 by the NABI-CORE grant to AKP and partial support from DST-SERB grant

743 (PDF/2016/001355) to PG. GK and AK acknowledge NABI-SRF Fellowships. Technical  
744 help from Jagdeep Singh for the GC-MS analysis is highly appreciated. DBT-eLibrary  
745 Consortium (DeLCON) is acknowledged for providing timely support and access to e-  
746 resources for this work. The wheat genome resources developed by International Wheat  
747 Genome Sequencing Consortium are highly appreciated. We also acknowledge the critical  
748 comments given by Dr. Kerry Pedley, USDA, USA. We would like to thank Abhijeet Panwar  
749 (CDAC-Pune) for his help in the preparation of the Sankey plot.

## Reference

- Aggarwal S, Kumar A, Bhati KK, Kaur G, Shukla V, Tiwari S, Pandey AK.** 2018. RNAi-mediated downregulation of inositol pentakisphosphate kinase (IPK1) in wheat grains decreases phytic acid levels and increases Fe and Zn accumulation. *Frontiers in Plant Science* **9**, 259.
- Bashir K, Hanada K, Shimizu M, Seki M, Nakanishi H and Nishizawa NK.** 2014. Transcriptomic analysis of rice in response to iron deficiency and excess. *Rice* **7**, 18.
- Bashir K, Nagasaka S, Itai RN, Kobayashi T, Takahashi M, Nakanishi H, Mori S, Nishizawa NK.** 2007. Expression and enzyme activity of glutathione reductase is upregulated by Fe-deficiency in graminaceous plants. *Plant Molecular Biology* **65**, 277–84.
- Bauer P, Blondet E.** 2011. Transcriptome analysis of *ein3 eil1* mutants in response to iron deficiency. *Plant Signaling & Behavior* **6**, 1669–1671.
- Beasley JT, Bonneau JP, Johnson AAT.** 2017. Characterisation of the nicotianamine aminotransferase and deoxymugineic acid synthase genes essential to Strategy II iron uptake in bread wheat (*Triticum aestivum* L.) *PLoS ONE* **12**, e0177061.
- Bhati KK, Alok A, Kumar A, Kaur J, Tiwari S, Pandey AK.** 2016. Silencing of *ABCC13* transporter in wheat reveals its involvement in grain development, phytic acid accumulation and lateral root formation. *Journal of Experimental Botany* **67**, 4379–4389.
- Bocchini M, Bartucca ML, Ciancaleoni S, Mimmo T, Cesco S, Pii Y, Albertini E, Del Buono D.** 2015. Iron deficiency in barley plants: phytosiderophore release, iron translocation, and DNA methylation. *Frontiers in Plant Science* **6**, 514.
- Borlotti A, Vignani G, Zocchi G.** 2012. Iron deficiency affects nitrogen metabolism in cucumber (*Cucumis sativus* L.) plants. *BMC Plant Biology* **12**, 189.

- Borrill P, Adamski N and Uauy C.** 2015. Genomics as the key to unlocking the polyploid potential of wheat. *New Phytologist* **208**, 1008-1022.
- Borrill P, Harrington SA, Uauy C.** 2018. Applying the latest advances in genomics and phenomics for trait discovery in polyploid wheat. *The Plant Journal* **97**, 56-72.
- Bouain N, Krouk G, Lacombe B, Rouached H.** 2019. Getting to the root of plant mineral nutrition: combinatorial nutrient stresses reveal emergent properties. *Trends in Plant Science* **24**, 542-552
- Buchner P, Hawkesford MJ.** 2014. Complex phylogeny and gene expression patterns of members of the NITRATE TRANSPORTER 1/PEPTIDE TRANSPORTER family (NPF) in wheat. *Journal of Experimental Botany* **65**, 5697–710.
- Buckhout TJ, Yang TJ, Schmidt W.** 2009. Early iron-deficiency-induced transcriptional changes in Arabidopsis roots as revealed by microarray analyses. *BMC Genomics* **10**, 147.
- Cataldo DA, Maroon M, Schrader LE, Youngs VL.** 1975. Rapid colorimetric determination of nitrate in plant tissue by nitration of salicylic acid. *Communications in Soil Science and Plant Analysis* **6**, 71–80.
- Colangelo EP, Guerinot ML.** 2004. The essential Basic Helix-Loop-Helix protein FIT1 is required for the iron deficiency response. *The Plant Cell* **16**, 3400–3412.
- Connorton JM, Balk J, Rodríguez-Celma J.** 2017. Iron homeostasis in plants – a brief overview. *Metallomics* **9**, 813–823.
- Connorton JM, Jones ER, Rodríguez-Ramiro I, Fairweather-Tait S, Uauy C, Balk J.** 2017. Wheat vacuolar iron transporter TaVIT2 transports Fe and Mn and is effective for biofortification. *Plant Physiology* **174**, 2434–2444.
- Curie C, Panaviene Z, Loulergue C, Dellaporta SL, Briat JF, Walker EL.** 2001. Maize yellow stripe1 encodes a membrane protein directly involved in Fe(III) uptake. *Nature* **409**, 346–349.
- Devaiah BN, Karthikeyan AS, Raghothama KG.** 2007. WRKY75 transcription factor is a modulator of phosphate acquisition and root development in Arabidopsis. *Plant Physiology* **143**, 1789–1801.
- Dixon DP, Davis BG, Edwards R.** 2002. Functional divergence in the glutathione transferase superfamily in plants. *Journal of Biological Chemistry* **277**, 30859–30869.
- Frieri I, Wirtz M and Hell R.** 2013. Toward new perspectives on the interaction of iron and sulfur metabolism in plants. *Frontiers in Plant Science* **4**, 357.

- Garnica M, Bacaicoa E, Mora V, San Francisco S, Baigorri R, Zamarreño AM, Garcia-Mina JM.** 2018. Shoot iron status and auxin are involved in iron deficiency-induced phytosiderophores release in wheat. *BMC Plant Biology* **18**, 105.
- Grillet L, Ouerdane L, Flis P, Hoang MTT, Isaure MP, Lobinski R, Curie C and Mari S.** 2014. Ascorbate efflux as a new strategy for iron reduction and transport in plants. *Journal of Biological Chemistry* **289**, 2515-2525.
- Gross J, Stein RJ, Fett-Neto AG, Fett JP.** 2003. Iron homeostasis related genes in rice. *Genetics and Molecular Biology* **26**, 477-497.
- Hell R, Stephan UW.** 2003. Iron uptake, trafficking and homeostasis in plants. *Planta* **216**, 541-51.
- Hindt MN, Guerinot ML.** 2012. Getting a sense for signals: regulation of the plant iron deficiency response. *Biochimica et Biophysica Acta* **1823**, 1521-30.
- Inoue H, Kobayashi T, Nozoye T, Takahashi M, Kakei Y, Suzuki K, Nakazono M, Nakanishi H, Mori S, Nishizawa NK.** 2009. Rice OsYSL15 is an iron-regulated iron (III)-deoxymugineic acid transporter expressed in the roots and is essential for iron uptake in early growth of the seedlings. *The Journal of Biological Chemistry* **284**, 3470-9.
- Ishimaru Y, Suzuki M, Tsukamoto T, et al.** 2006. Rice plants take up iron as an Fe<sup>3+</sup> -phytosiderophore and as Fe<sup>2+</sup>. *The Plant Journal* **45**, 335-346.
- Ivanov R, Brumbarova T, Bauer P.** 2012. Fitting into the harsh reality: regulation of iron-deficiency responses in dicotyledonous plants. *Molecular Plant* **5**, 27-42.
- Jakoby M, Wang HY, Reidt W, Weisshaar B, Bauer P.** 2004. *FRU (BHLH029)* is required for induction of iron mobilization genes in *Arabidopsis thaliana*. *FEBS Letters* **577**, 528-534.
- Kabir AH, Paltridge NG, Roessner U, Stangoulis JCR.** 2013. Mechanisms associated with Fe-deficiency tolerance and signaling in shoots of *Pisum sativum*. *Physiologia Plantarum* **147**, 381-395.
- Kim J, Rees DC.** 1992. Structural models for the metal centers in the nitrogenase molybdenum-iron protein. *Science* **257**, 1677-82.
- Kim MJ, Ruzicka D, Shin R, Schachtman DP.** 2012. The Arabidopsis AP2/ERF transcription factor RAP2.11 modulates plant response to low-potassium conditions. *Molecular Plant* **5**, 1042-1057.
- Kim SA, Punshon T, Lanzirotti A, Li L, Alonso JM, Ecker JR, Kaplan J, Guerinot ML.** 2006. Localization of iron in Arabidopsis seed requires the vacuolar membrane transporter VIT1. *Science* **314**, 1295-1298.

- Kispal G, Csere P, Guiard B, Lill R.** 1997. The ABC transporter Atm1p is required for mitochondrial iron homeostasis. *FEBS Letters* **418**, 346–50.
- Kobayashi K, Baba S, Obayashi T, et al.** 2012. Regulation of root greening by light and auxin/cytokinin signaling in *Arabidopsis*. *The Plant Cell* **24**, 1081–1095.
- Kobayashi K, Sasaki D, Noguchi K, et al.** 2013. Photosynthesis of root chloroplasts developed in *Arabidopsis* lines overexpressing GOLDEN2-LIKE transcription factors. *Plant and Cell Physiology* **54**, 1365–1377.
- Kobayashi T, Itai RN, Ogo Y, Kakei Y, Nakanishi H, Takahashi M, Nishizawa NK.** 2009. The rice transcription factor IDEF1 is essential for the early response to iron deficiency, and induces vegetative expression of late embryogenesis abundant genes. *The Plant Journal* **60**, 948–961.
- Kobayashi T, Nakanishi Itai R, Nishizawa NK.** 2014. Iron deficiency responses in rice roots. *Rice* **7**, 27.
- Kobayashi T, Nishizawa NK.** 2012. Iron uptake, translocation, and regulation in higher plants. *Annual Review of Plant Biology* **63**, 131–152.
- Kumar A, Kaur G, Goel P, Bhati KK, Kaur M, Shukla V, Pandey AK.** 2019. Genome-wide analysis of oligopeptide transporters and detailed characterization of yellow stripe transporter genes in hexaploid wheat. *Functional & Integrative Genomics* **19**, 75-90.
- Kumar S, Trivedi PK.** 2018. Glutathione S-Transferases: role in combating abiotic stresses including arsenic detoxification in plants. *Frontiers in Plant Science* **9**, 751.
- Leach LJ, Belfield EJ, Jiang C, Brown C, Mithani A and Harberd NP.** 2014. Patterns of homoeologous gene expression shown by RNA sequencing in hexaploid bread wheat. *BMC Genomics* **15**, 276.
- Lee S, Chiecko JC, Kim SA, Walker EL, Lee Y, Guerinot ML, An G.** 2009. Disruption of OsYSL15 leads to iron inefficiency in rice plants. *Plant Physiology* **150**, 786–800.
- Li W, Lan P.** 2017. The understanding of the plant iron deficiency responses in strategy I plants and the role of ethylene in this process by omic approaches. *Frontiers in Plant Science* **8**, 40.
- Li X, Zhang H, Ai Q, Liang G, Yu D.** 2016. Two bHLH transcription Factors, bHLH34 and bHLH104, regulate iron homeostasis in *Arabidopsis thaliana*. *Plant Physiology* **170**, 2478–2493.
- Li Y, Wang N, Zhao F, Song X, Yin Z, Huang R, Zhang C.** 2014. Changes in the transcriptomic profiles of maize roots in response to iron-deficiency stress. *Plant Molecular Biology* **85**, 349–363.

- Lin XY, Ye YQ, Fan SK, Jin CW, Zheng SJ.** 2016. Increased sucrose accumulation regulates iron-deficiency responses by promoting auxin signaling in arabidopsis plants. *Plant Physiology* **170**, 907–920.
- Liu Z, Xin M, Qin J, Peng H, Ni Z, Yao Y, Sun Q.** 2015. Temporal transcriptome profiling reveals expression partitioning of homeologous genes contributing to heat and drought acclimation in wheat (*Triticum aestivum* L.). *BMC Plant Biology* **15**, 152.
- Lohse M, Nagel A, Herter T, May P, Schroda M, Zrenner R, Tohge T, Fernie AR, Stitt M, Usadel B.** 2014. Mercator: a fast and simple web server for genome scale functional annotation of plant sequence data. *Plant, Cell & Environment* **37**, 1250–1258.
- Long TA, Tsukagoshi H, Busch W, Lahner B, Salt DE, Benfey PN.** 2010. The bHLH transcription factor POPEYE regulates response to iron deficiency in Arabidopsis roots. *The Plant Cell* **22**, 2219–2236.
- Ma JF, Taketa S, Chang YC, Takeda K and Matsumoto H.** 1999. Biosynthesis of phytosiderophores in several *Triticeae* species with different genomes. *Journal of Experimental Botany* **50**, 723-726.
- Maere S, Heymans K, Kuiper M.** 2005. BiNGO: a Cytoscape plugin to assess overrepresentation of gene ontology categories in biological networks. *Bioinformatics* **21**, 3448–3449.
- Mai HJ, Pateyron S, Bauer P.** 2016. Iron homeostasis in Arabidopsis thaliana: transcriptomic analyses reveal novel FIT-regulated genes, iron deficiency marker genes and functional gene networks. *BMC Plant Biology* **16**, 211.
- Marschner H.** 1995. Mineral nutrition of higher plants. Second edition. Academic Press Edition London.
- Mayer KFX, Rogers J, Dole el J, et al.** 2014. A chromosome-based draft sequence of the hexaploid bread wheat (*Triticum aestivum*) genome. *Science* **345**, 1251788–1251788.
- Merico D, Isserlin R, Stueker O, Emili A, Bader GD.** 2010. Enrichment Map: A network-based method for gene-set enrichment visualization and interpretation. *PLoS ONE* **5**, e13984.
- Mori S.** 1999. Iron acquisition by plants. *Current Opinion in Plant Biology* **2**, 250–253.
- Morrissey J, Guerinot ML.** 2009. Iron uptake and transport in plants: the good, the bad, and the ionome. *Chemical Reviews* **109**, 4553–4567.
- Nishizawa NK.** 2007. Expression and enzyme activity of glutathione reductase is upregulated by Fe-deficiency in graminaceous plants. *Plant Molecular Biology* **65**, 277–84.

- Nozoye T, Nagasaka S, Kobayashi T, Sato Y, Uozumi N, Nakanishi H, Nishizawa NK.** 2015. The Phytosiderophore efflux transporter TOM2 is involved in metal transport in rice. *Journal of Biological Chemistry* **290**, 27688–27699.
- Nozoye T, Nagasaka S, Kobayashi T, Takahashi M, Sato Y, Sato Y, Uozumi N, Nakanishi H, Nishizawa NK.** 2011. Phytosiderophore efflux transporters are crucial for iron acquisition in graminaceous plants. *Journal of Biological Chemistry* **286**, 5446–5454.
- Ogo Y, Itai RN, Kobayashi T, Aung MS, Nakanishi H, Nishizawa NK.** 2011. OsIRO2 is responsible for iron utilization in rice and improves growth and yield in calcareous soil. *Plant Molecular Biology* **75**, 593–605.
- Ogo Y, Nakanishi Itai R, Nakanishi H, Kobayashi T, Takahashi M, Mori S, Nishizawa NK.** 2007. The rice bHLH protein OsIRO2 is an essential regulator of the genes involved in Fe uptake under Fe-deficient conditions. *The Plant Journal* **51**, 366–377.
- Palmer CM, Hindt MN, Schmidt H, Clemens S and Guerinot ML.** 2013. MYB10 and MYB72 are required for growth under iron-limiting conditions. *PLoS Genetics* **9**, 1003953.
- Palmer L, Dias D, Boughton B, Roessner U, Graham R, Stangoulis JC.** 2014. Metabolite profiling of wheat (*Triticum aestivum* L.) phloem exudate. *Plant Methods* **10**, 27.
- Powell JJ, Fitzgerald TL, Stiller J, Berkman PJ, Gardiner DM, Manners JM, Henry RJ, Kazan K.** 2017. The defence-associated transcriptome of hexaploid wheat displays homoeolog expression and induction bias. *Plant Biotechnology Journal* **15**, 533–543.
- Quanbeck SM, Brachova L, Campbell AA, et al.** 2012. Metabolomics as a hypothesis-generating functional genomics tool for the annotation of *Arabidopsis thaliana* genes of “Unknown Function”. *Frontiers in Plant Science* **3**, 15.
- Quinet M, Vromman D, Clippe A, Bertin P, Lequeux H, Dufey I, Lutts S and Lefevre I.** 2012. Combined transcriptomic and physiological approaches reveal strong differences between short- and long-term response of rice (*Oryza sativa*) to iron toxicity. *Plant, Cell & Environment* **35**, 1837-1859.
- Ramírez L, Bartoli CG, Lamattina L.** 2013. Glutathione and ascorbic acid protect *Arabidopsis* plants against detrimental effects of iron deficiency. *Journal of Experimental Botany* **64**, 3169–78.
- Ramírez-González RH, Borrill P, Lang D, et al.** 2018. The transcriptional landscape of polyploid wheat. *Science* **361**, 6089.
- Romera FJ, Alcantara E.** 1994. Iron-deficiency stress responses in cucumber (*Cucumis sativus* L.) roots (a possible role for ethylene?). *Plant Physiology* **105**, 1133–1138.

- Romera FJ, García MJ, Alcántara E, Pérez-Vicente R.** 2011. Latest findings about the interplay of auxin, ethylene and nitric oxide in the regulation of Fe deficiency responses by Strategy I plants. *Plant Signaling & Behavior* **6**, 167–70.
- Rouached H, Rhee SY.** 2017. System-level understanding of plant mineral nutrition in the big data era. *Current Opinion in Systems Biology* **4**, 71–77.
- Rubio V.** 2001. A conserved MYB transcription factor involved in phosphate starvation signaling both in vascular plants and in unicellular algae. *Genes & Development* **15**, 2122–2133.
- Santi S, Cesco S, Varanini Z, Pinton R.** 2005. Two plasma membrane H<sup>+</sup>-ATPase genes are differentially expressed in iron-deficient cucumber plants. *Plant Physiology and Biochemistry* **43**, 287–292.
- Santi S, Schmidt W.** 2009. Dissecting iron deficiency-induced proton extrusion in Arabidopsis roots. *New Phytologist* **183**, 1072–1084.
- Schaaf G, Ludewig U, Erenoglu BE, Mori S, Kitahara T, von Wirén N.** 2004. ZmYS1 functions as a proton-coupled symporter for phytosiderophore- and nicotianamine-chelated metals. *Journal of Biological Chemistry* **279**, 9091–9096.
- Schaedler TA, Thornton JD, Kruse I, Schwarzländer M, Meyer AJ, van Veen HW, Balk J.** 2014. A conserved mitochondrial ATP-binding cassette transporter exports glutathione polysulfide for cytosolic metal cofactor assembly. *Journal of Biological Chemistry* **289**, 23264–23274.
- Schmidt H, Günther C, Weber M, Spörlein C, Loscher S, Böttcher C, Schobert R and Clemens S.** 2014. Metabolome analysis of Arabidopsis thaliana roots identifies a key metabolic pathway for iron acquisition. *PloS ONE* **9**, 102444.
- Schmidt W, Tittel J, Schikora A.** 2000. Role of hormones in the induction of iron deficiency responses in Arabidopsis roots. *Plant Physiology* **122**, 1109–18.
- Shanmugam V, Wang Y-W, Tsednee M, Karunakaran K, Yeh K-C.** 2015. Glutathione plays an essential role in nitric oxide-mediated iron-deficiency signaling and iron-deficiency tolerance in Arabidopsis. *The Plant Journal* **84**, 464–77.
- Shukla D, Rinehart CA, Sahi SV.** 2017. Comprehensive study of excess phosphate response reveals ethylene mediated signaling that negatively regulates plant growth and development. *Scientific Reports* **7**, 3074.
- Sipos K, Lange H, Fekete Z, Ullmann P, Lill R, Kispal G.** 2002. Maturation of cytosolic iron-sulfur proteins requires glutathione. *The Journal of Biological Chemistry* **277**, 26944–9.

- Sperotto RA, Vasconcelos MW, Grusak MA, Fett JP.** 2012. Effects of different Fe supplies on mineral partitioning and remobilization during the reproductive development of rice (*Oryza sativa* L.). *Rice* **5**, 27.
- Takagi SI.** 1976. Naturally occurring iron-chelating compounds in oat-and rice-root washings: I. Activity measurement and preliminary characterization. *Soil Science and Plant Nutrition* **22**, 423-433.
- Terzano R, Mimmo T, Vekemans B, Vincze L, Falkenberg G, Tomasi N, Ramos MS, Pinton R and Cesco S.** 2013. Iron (Fe) speciation in xylem sap by XANES at a high brilliant synchrotron X-ray source: opportunities and limitations. *Analytical and Bioanalytical Chemistry* **405**, 5411-5419.
- Thimm O, Bläsing O, Gibon Y, Nagel A, Meyer S, Krüger P, Selbig J, Müller LA, Rhee SY, Stitt M.** 2004. MAPMAN: a user-driven tool to display genomics data sets onto diagrams of metabolic pathways and other biological processes. *The Plant Journal* **37**, 914–39.
- Thimm O, Essigmann B, Kloska S, Altmann T, Buckhout TJ.** 2001. Response of Arabidopsis to iron deficiency stress as revealed by microarray analysis. *Plant Physiology* **127**, 1030–43.
- Thomine S, Vert G.** 2013. Iron transport in plants: better be safe than sorry. *Current Opinion in Plant Biology* **16**, 322–7.
- Tolay I, Erenoglu B, Römheld V, Braun HJ, Cakmak I.** 2001. Phytosiderophore release in *Aegilops tauschii* and *Triticum* species under zinc and iron deficiencies. *Journal of Experimental Botany* **52**, 1093–9.
- Wagner DS, Pirhalla JL, Bowers GD.** 2013. Metabolite structure analysis by high-resolution MS: supporting drug-development studies. *Bioanalysis* **5**, 463–479.
- Wang Y, Lysøe E, Armarego-Marriott T, Erban A, Paruch L, van Eerde A, Bock R, Liu-Clarke J.** 2018. Transcriptome and metabolome analyses provide insights into root and root-released organic anion responses to phosphorus deficiency in oat. *Journal of Experimental Botany* **69**, 3759–3771.
- Waters BM, Sankaran RP.** 2011. Moving micronutrients from the soil to the seeds: Genes and physiological processes from a biofortification perspective. *Plant Science* **180**, 562–574.
- Xie C, Mao X, Huang J, Ding Y, Wu J, Dong S, Kong L, Gao G, Li C-Y, Wei L.** 2011. KOBAS 2.0: a web server for annotation and identification of enriched pathways and diseases. *Nucleic Acids Research* **39**, W316-22.

- Yang TJW, Lin WD, Schmidt W.** 2010. Transcriptional profiling of the Arabidopsis iron deficiency response reveals conserved transition metal homeostasis networks. *Plant Physiology* **152**, 2130–2141.
- Yordem BK, Conte SS, Ma JF, Yokosho K, Vasques KA, Gopalsamy SN, Walker EL.** 2011. *Brachypodium distachyon* as a new model system for understanding iron homeostasis in grasses: phylogenetic and expression analysis of Yellow Stripe-Like (YSL) transporters. *Annals of Botany* **108**, 821–833.
- Yousfi S, Rabhi M, Abdelly C, Gharsalli M.** 2009. Iron deficiency tolerance traits in wild (*Hordeum maritimum*) and cultivated barley (*Hordeum vulgare*). *Comptes Rendus Biologies* **332**, 523–533.
- Zanin L, Venuti S, Zamboni A, Varanini Z, Tomasi N, Pinton R.** 2017. Transcriptional and physiological analyses of Fe deficiency response in maize reveal the presence of Strategy I components and Fe/P interactions. *BMC Genomics* **18**, 154.
- Zhang Y, Liu J, Zhou Y, Gong T, Wang J, Ge Y.** 2013. Enhanced phytoremediation of mixed heavy metal (mercury)–organic pollutants (trichloroethylene) with transgenic alfalfa co-expressing glutathione S-transferase and human P450 2E1. *Journal of Hazardous Materials* **260**, 1100–1107.
- Zheng L, Huang F, Narsai R, et al.** 2009. Physiological and transcriptome analysis of iron and phosphorus interaction in rice seedlings. *Plant Physiology* **151**, 262–274.
- Zuchi S, Watanabe M, Hubberten H-M, et al.** 2015. The interplay between sulfur and iron nutrition in tomato. *Plant Physiology* **169**, 2626–2639.

**Table 1:** Metal concentration (mg/g of tissue dry weight) in roots and shoots of wheat seedlings subjected to –Fe stress.

<i>Treatme nts</i>	ROOTS					SHOOTS				
	Fe	Zn	Mn	Mg	Cu	Fe	Zn	Mn	Mg	Cu
<b>+Fe+P</b>	106.73 ± 14.2	14.6 ± 3.2	15.8 ± 2.0	542 ± 70	7.4 ± 1.1	72.9 ± 1.7	26.8 ± .09	17.4 ± .05	1031 ± 2.3	10.4 ± 0.6
<b>–Fe +P</b>	66.8 ± 17	<b>40.4 ±</b> 12	<b>38.2 ±</b> 8.9	<b>912 ±</b> 213	<b>17.9 ±</b> 3.7	28.6 ± 1.6	22.3 ± 1.05	22.1 ± 1.9	1013 ± 48	5.1 ± 0.3

**Table 2:** List of genes showing genome induction bias contribution from either A or B sub-genome. Expression changes within triads w.r.t. iron stress were observed to identify the presence of differential regulation among homoeologs from each triad, thus contributing towards genome induction bias. Table gives descriptive list of homoeologs that were up/down-regulated under iron starvation only in the A sub-genome, followed by those only in the B sub-genome.

Gene	logFold change	RAP-DB description
<b>A genome</b>		
TRIAE_CS42_3AL_TGACv1_197291_AA0665720	3.01	Myb transcription factor domain containing protein.
TRIAE_CS42_2AL_TGACv1_094922_AA0304900	2.8	Similar to Prolyl endopeptidase (EC 3.4.21.26) (Post-proline cleaving enzyme) (PE).
TRIAE_CS42_5AL_TGACv1_379416_AA1256390	2.44	Similar to Solute carrier family 35, member F1.
TRIAE_CS42_2AL_TGACv1_094606_AA0300340	2.18	RmlC-like jelly roll fold domain containing protein.
TRIAE_CS42_3AS_TGACv1_211026_AA0683370	3.36	Protein of unknown function DUF1399 family protein.
TRIAE_CS42_7AL_TGACv1_557470_AA1781720	3.47	Heavy metal-transporting PIB-ATPase, Root-to-shoot cadmium (Cd) translocation
TRIAE_CS42_6AL_TGACv1_471682_AA1512850	2.26	Similar to CRT/DRE binding factor 1.
TRIAE_CS42_6AS_TGACv1_485332_AA1543320	1.85	Zinc/iron permease family protein.
TRIAE_CS42_2AL_TGACv1_092944_AA0267670	2.43	Heavy metal transport/detoxification protein domain containing protein.
TRIAE_CS42_5AL_TGACv1_375378_AA1220660	2.21	Similar to SUSIBA2 (WRKY protein).
TRIAE_CS42_1AL_TGACv1_000708_AA0017440	2.57	Chlorophyll a-b binding protein 2, chloroplast precursor (LHCII type I CAB-2) (LHCP).
TRIAE_CS42_2AL_TGACv1_093154_AA0273510	1.86	C2 domain containing protein.
TRIAE_CS42_5AL_TGACv1_374025_AA1188170	2.66	Nodulin-like domain containing protein.
TRIAE_CS42_3AL_TGACv1_197522_AA0666570	2.22	Lipase, GDSL domain containing protein.
TRIAE_CS42_7AL_TGACv1_556100_AA1755640	2.34	Bifunctional inhibitor/plant lipid transfer protein/seed storage domain containing protein.
TRIAE_CS42_4AS_TGACv1_306527_AA1009640	2.2	Multi antimicrobial extrusion protein MatE family protein.
TRIAE_CS42_7AS_TGACv1_570336_AA1834060	1.98	Major facilitator superfamily protein.
TRIAE_CS42_2AL_TGACv1_093456_AA0280470	2.15	Glycolipid transfer protein domain domain containing protein.
TRIAE_CS42_1AL_TGACv1_002205_AA0039730	-2.09	Similar to IAA8 (Fragment).

TRIAE_CS42_4AL_TGACv1_290815_AA0989640	-2	Lipase, class 3 family protein.
TRIAE_CS42_5AL_TGACv1_374561_AA1203290	-2.24	Cinnamyl alcohol dehydrogenase (EC 1.1.1.195).
TRIAE_CS42_5AL_TGACv1_374359_AA1197930	-2.36	Similar to Lipoyxygenase L-2 (EC 1.13.11.12).
TRIAE_CS42_6AL_TGACv1_472625_AA1524260	-1.89	RAG1-activating protein 1 homologue domain containing protein.
TRIAE_CS42_7AL_TGACv1_558250_AA1791610	-2.32	Similar to Pleiotropic drug resistance protein 3.
TRIAE_CS42_2AL_TGACv1_097246_AA0323500	-1.72	Similar to Peroxidase (EC 1.11.1.7).
TRIAE_CS42_7AL_TGACv1_556210_AA1758330	-2.21	Similar to Kaurene synthase A (Fragment).
TRIAE_CS42_1AL_TGACv1_000555_AA0014640	-1.84	No apical meristem (NAM) protein domain containing protein.
TRIAE_CS42_6AL_TGACv1_471077_AA1502240	-1.79	Similar to OSIGBa0145M07.8 protein.
TRIAE_CS42_7AL_TGACv1_559906_AA1801190	-1.68	Similar to H0801D08.12 protein.
TRIAE_CS42_7AL_TGACv1_558101_AA1790150	-1.76	Similar to Acyl-ACP thioesterase (Fragment).
TRIAE_CS42_6AL_TGACv1_472321_AA1520860	-2.06	Similar to Subtilisin-like protease (Fragment).
<b>B Genome</b>		
TRIAE_CS42_5BS_TGACv1_423346_AA1374840	2.19	Similar to Calmodulin NtCaM13.
TRIAE_CS42_3B_TGACv1_224030_AA0791180	2.2	Similar to IN2-2 protein.
TRIAE_CS42_2BL_TGACv1_129296_AA0377070	2.46	Similar to OSIGBa0127A14.7 protein.
TRIAE_CS42_6BL_TGACv1_499646_AA1588130	2.32	TGF-beta receptor, type I/II extracellular region family protein.
TRIAE_CS42_7BS_TGACv1_592587_AA1940840	2.25	Similar to RING-H2 finger protein ATL1R (RING-H2 finger protein ATL8).
TRIAE_CS42_2BS_TGACv1_146290_AA0461590	2.64	NA
TRIAE_CS42_5BL_TGACv1_404610_AA1306090	1.84	Similar to Senescence-associated protein SAG102.
TRIAE_CS42_5BL_TGACv1_405319_AA1324840	2.77	Similar to Transporter associated with antigen processing-like protein.
TRIAE_CS42_7BL_TGACv1_577614_AA1879540	2.69	Peptidase A1 domain containing protein.
TRIAE_CS42_4BS_TGACv1_329166_AA1098520	2.32	Similar to Alcohol dehydrogenase.
TRIAE_CS42_4BL_TGACv1_321683_AA1064050	2.56	Protein of unknown function DUF1262 family protein.
TRIAE_CS42_7BL_TGACv1_591489_AA1920550	NA	Similar to zinc transporter 4.
TRIAE_CS42_7BL_TGACv1_577301_AA1871590	2.41	Delta-tonoplast intrinsic protein.
TRIAE_CS42_4BS_TGACv1_329309_AA1100040	NA	Similar to Major facilitator superfamily antiporter.
TRIAE_CS42_2BL_TGACv1_129348_AA0379680	2	Hypothetical conserved gene.
TRIAE_CS42_2BS_TGACv1_148847_AA0495340	4.34	Helix-loop-helix DNA-binding domain containing protein.
TRIAE_CS42_2BL_TGACv1_130820_AA0418390	1.88	NA
TRIAE_CS42_1BL_TGACv1_031794_AA0120680	-2.79	Divalent ion symporter domain containing protein.
TRIAE_CS42_5BL_TGACv1_406838_AA1350360	-2.29	Similar to anther-specific proline-rich protein APG.
TRIAE_CS42_2BL_TGACv1_130182_AA0405730	-2.09	Protein of unknown function DUF3741 domain containing protein.
TRIAE_CS42_4BS_TGACv1_330685_AA1108490	-2.83	Serine/threonine protein kinase-related domain containing protein.
TRIAE_CS42_2BS_TGACv1_147909_AA0488910	-2.28	Delayed-early response protein/equilibrative nucleoside transporter family protein.
TRIAE_CS42_3B_TGACv1_224656_AA0799480	-1.83	Glyoxalase/bleomycin resistance protein/dioxygenase domain containing protein.
TRIAE_CS42_7BL_TGACv1_577476_AA1876230	-2.93	Protein kinase, catalytic domain domain containing protein.
TRIAE_CS42_6BL_TGACv1_499809_AA1592210	-1.88	Cupredoxin domain containing protein.
TRIAE_CS42_7BL_TGACv1_576755_AA1853830	-2.04	Cellulase (EC 3.2.1.4).

TRIAE_CS42_2BL_TGACv1_130686_AA0416110	-2.3	Similar to OSIGBa0096P03.3 protein.
TRIAE_CS42_2BS_TGACv1_146035_AA0453750	NA	Conserved hypothetical protein.
TRIAE_CS42_1BL_TGACv1_030699_AA0098220	-1.91	Lipase, class 3 family protein.
TRIAE_CS42_2BL_TGACv1_129634_AA0391150	-1.78	2OG-Fe(II) oxygenase domain containing protein.

**Table 3:** Percentage of homoeolog triads categorised into ideal genome expression bias categories in control and Fe starved conditions.

	<b>Control</b>	<b>-Fe</b>
<b>Balanced</b>	77.07%	77.89%
<b>A-suppressed</b>	6.90%	6.90%
<b>B-suppressed</b>	7.09%	6.82%
<b>D-suppressed</b>	5.15%	4.93%
<b>A-dominant</b>	1.12%	0.94%
<b>B-dominant</b>	1.24%	1.18%
<b>D-dominant</b>	1.43%	1.32%

### Legends for Figures:

**Fig. 1.** Effect of Fe-starvation (-Fe) on the growth parameters of wheat seedlings post 20 days after starvation. (A) Phenotype of wheat seedlings exposed to Fe starvation. (B) Total biomass of roots and shoots of wheat seedlings after 20 DAS. 12-15 seedlings were collected for calculating the fresh tissue weight (in grams). (C) Number of first order lateral roots in roots subjected to -Fe condition and control plants (+Fe). (D) Primary root length of wheat roots. 10-12 seedlings were used for measuring the total primary root length of wheat seedlings under -Fe and +Fe condition. # indicate significant difference at  $p < 0.05$ .

**Fig. 2.** Analysis of RNAseq data from the wheat roots during Fe starvation. (A) Principal component analysis of samples from control (Control\_0, Control\_1) and -Fe (Single1\_0, Single1\_1) conditions. (B) Volcano plot of DEGs, the x-axis shows the log<sub>2</sub> fold change difference in the expression of genes in iron starved condition w.r.t. control, and the y-axis indicates the negative log of p-value (pval) for the differences in expression. Genes without significant differences are indicated by grey dots. Significant genes with logFC > 0 are represented by red dots, and those with logFC < 0 are represented by green dots in the scatter plot. (C) Number of DEGs in -Fe. Up: Upregulated under -Fe (logFC > 1), Down: Downregulated under -Fe (logFC < -1), Exc-Fe: exclusively expressed in -Fe, ExcCtrl: Exclusively expressed in control condition.

**Fig. 3.** Genomic distribution and homoeolog bias studies during Fe starvation. (A) Chromosomal inclination of DEGs. (B) Pie charts showing (left panel) sub-genomic distribution of genome induction bias in triads where one of the homoeologs was up/down-regulated. A, B and D depict the sub-genome to which the DE homoeolog belongs; (right Panel) distribution of triads for which two of the homoeologs were differentially expressed and the third one had normal expression. AB refers to the triads for which up/down regulation was observed in the homoeologs belonging to A and B sub-genomes, while the D sub-genome homoeolog behaved normal w.r.t control. (C) Sankey diagram depicting the homoeolog expression bias in Control condition and Fe starvation. Homoeolog triads were classified into the defined seven categories based on relative normalised expression within each triad. Nodes flowing from Control to -Fe (Fe starvation) represent the triads with same (flow to same category) as well as changed (flow to a different category) expression patterns across both conditions. Distinct colors represent the flow of triads belonging to the seven categories from control condition into same category under -Fe or transition into a different category under -Fe.

**Fig. 4.** Top up-regulated and down-regulated genes in -Fe condition, annotated via KOBAS using rice RAP-DB/RefSeq annotations as reference. The heat map shows top 50 genes those are highly up-regulated (red-left panel) and down-regulated (green-right panel) identified in wheat roots under -Fe condition with respect to control. For expression analysis, FPKM values were obtained using Cufflinks, and CuffDiff was used to identify DEGs by calculating significant changes in transcript expression between the stressed and normal samples ( $FDR \leq 0.05$ ).

**Fig. 5.** Gene ontology (GO) categorization of the differentially expressed genes and its analysis. (A) WEGO plot describing GO annotation and classification of DEGs, with y-axis showing the percentage of genes belonging to respective GO terms (grey bars for down-regulated genes and red bars for up-regulated genes) as well as the right plane ticks for y-axis depicting the number of both up- and down-regulated genes represented by the respective percentages on the left plane. Percentage and number of genes were calculated for the three broad main categories listed on the x-axis; (B) Enriched GO terms in DEGs under -Fe condition, y-axis depicting the significance of GO term enrichment. (C) Figure showing top 20 enriched KEGG pathways represented by the up-regulated genes under iron starvation condition. x-axis showing names of the pathways, y-axis representing the number of genes enriched in respective pathways.

**Fig. 6.** Co-expression/hub genes and function enrichment network for identified DEGs. Function enrichment network for DEGs associated under Iron starvation in wheat roots with high significance ( $FDR \leq 0.05$ ) for (A) Up-regulated and (B) Down-regulated genes. Enriched GO functional categories are clustered with correlated DEGs and represented by node circles.

**Fig. 7.** Transcriptional factors (TFs) significantly associated with Fe starvation ( $FDR \leq 0.05$ ) in wheat roots. (A) List of TFs differentially expressed in response to Fe starvation stress. Blue bars represent up-regulated and red bars represent down-regulated TFs. (B) Co-expression/hub genes and network analysis using Fe responsive TFs ( $FDR \leq 0.05$ ) in wheat roots. Circles indicate the processes associated with it (green for down-regulated genes; Blue for up-regulated genes). Enriched GO functional categories are clustered with correlated TFs and represented by node circles.

**Fig. 8.** Measurement of GST activity and metabolite profiling of wheat roots subjected to Fe starvation. (A) Glutathione-S-transferase activity of wheat roots under Fe starvation (-Fe) and control (+Fe) condition. (B) Metabolite profiling of amino acids, sugars, polyols, organic acids and related compounds. Change in abundance of significant ( $P < 0.05$ ) metabolites identified by GC-MS in Fe-starved roots. Abundance variation of each metabolite is represented in Log<sub>2</sub> fold values of response ratio (-Fe /+Fe) of metabolite concentrations. Values are means of three biological replicates with bar representing Log ratio of standard error. \* indicate significant difference at  $p < 0.01$ ; # indicate significant difference at  $p < 0.05$ .

**Fig. 9.** Schematic representation describing the core components involved in Fe starvation. The red font indicates the genes/metabolite those were highly up-regulated/showed high-accumulation during our study; whereas the green font indicates down-regulated/low accumulation. Methionine salvage pathway bins indicate the level of the gene expression levels for the transcript indicated next to it. Red and blue bins near pathways and steps represent the up- and down-regulation of related genes, respectively. (Abbreviation used: FBP: fructose-1,6-bisphosphatase I, PFP: diphosphate-dependent phosphofructokinase, ALDO: fructose-bisphosphate aldolase, GAPDH: glyceraldehyde 3-phosphate dehydrogenase, PGAM: 2,3-bisphosphoglycerate-dependent phosphoglycerate mutase, PDC: pyruvate decarboxylase, GLYK: D-glycerate 3-kinase, GlyA: glycine hydroxymethyltransferase, ltaE: threonine aldolase, BMT2: homocysteine S-methyltransferase, metE: homocysteine methyltransferase, metK: S-adenosylmethionine synthetase, SamDC: S-adenosylmethionine decarboxylase, SRM: spermidine synthase, MTN: 5'-methylthioadenosine nucleosidase, mtnK: 5-methylthioribose kinase, mtnA: methylthioribose-1-phosphate isomerase, DEP1: enolase-phosphatase E1, mtnC: enolase-phosphatase E1, mtnD: 1,2-dihydroxy-3-keto-5-methylthiopentene dioxygenase, TyrAT: tyrosine aminotransferase, NAS: nicotianamine synthase, NAAT: nicotianamine aminotransferase, DMAS: 3"-

deamino-3"-oxonicotianamine reductase, YSL: Yellow Stripe Like, maiA: maleylacetoacetate isomerase, AAT: aspartate aminotransferase, TAT: tyrosine aminotransferase, HPD: 4-hydroxyphenylpyruvate dioxygenase, GGT: gamma-glutamyltranspeptidase, AOS3: hydroperoxide dehydratase, OPR: 12-oxophytodienoic acid reductase, ACX: acyl-CoA oxidase, MFP2: enoyl-CoA hydratase, ACAT: acetyl-CoA acyltransferase 1)

## Supporting information

**Supplementary Fig. S1:** qRT-PCR validation of selected genes from the DEGs during Fe-deficient roots after 20 days of starvation. A total of 2 µg of RNA (DNA free) was used for cDNA synthesis and qRT-PCR was performed using gene specific primers (Supplementary Table S1).  $C_t$  values were normalized against wheat *ARF1* as an internal control.

**Supplementary Fig. S2:** Overview of genes modulated by the Fe starvation in wheat roots. MapMan overview demonstrating differentially expressed transcripts under iron starvation in general metabolic pathways. Log<sub>2</sub> fold change values of DEGs were imported into MapMan. Red and blue bins represent up-regulation and down-regulation, respectively, in terms of log<sub>2</sub> fold change, as shown by the scale.

**Supplementary Fig. S3:** MapMan visualization depicting the differentially expressed transcription factors families, with red and blue colored bins for up and down-regulated transcripts, respectively. Numbers in the scale represent fold changes in expression levels expressed as Log<sub>2</sub>.

**Supplementary Fig. S4:** Estimation of Nitrate levels under Fe-starvation using salicylic acid method. Three Biological replicate root samples of 10, 15 and 20 days after starvation (DAS) were completely dried for the extraction. Yellow coloration (in test tubes: lower panel) represents level of nitrate in the sample. Potassium Nitrate was used as standard in 0-70 µg concentrations.

**Supplementary Fig. S5:** Characterization of wheat ABCB25 transporter. (A) Phylogeny analysis of TaABCB25 along with its closest orthologs from rice and arabidopsis. (B) Expression analysis of *TaABCC25* in roots of wheat seedlings subjected to Fe starvation. Wheat seedlings (5-7 days old) were subjected to Fe stress and samples were harvested after 12 hours, 3, 6, 9 and 15 days(d) post starvation. The relative qRT-PCR was performed using wheat ADP-ribosylation factor (ARF) as an internal control gene. Fold accumulation was calculated with respect to the control roots. (C) Schematic comparison of different domains of AtABCB27, OsABCB25 and TaABC25. The number indicates the predicted amino acid position of the TM domains.

**Supplementary Table S1: List of primers used in the current study.** \*wheat genes named according to rice RAP-DB/RefSeq based on KOBAS annotation.

**Supplementary Table S2: Summary of filtered and mapped reads for each sample.** Obtained RNA-seq reads were quality filtered using Trimmomatic v0.35. TopHat was used to map the obtained reads to the wheat genome (TGACv1).

**Supplementary Table S3: DEGs in response to Fe starvation in wheat roots** List of up-regulated genes, downregulated genes (sheet 2), genes exclusively expressed in response to Fe starvation (sheet 3). Table enlists Control and Fe starvation expression values, logFC for Fe starvation wrt Control samples. Each DEG is annotated with information like rice ortholog, gene definition, KEGG Orthology, Pathways and Pfam domains, which were obtained through KOBAS 3.0 stand-alone tool, using *Oryza sativa* RAP-DB and RefSeq as reference.

**Supplementary Table S4: List of 8473 homoeolog triads that were used for homoeolog induction and expression biasness analysis.** 8473 homoeolog triplets that were expressed in A, B as well as, D genome were selected for homoeolog specific analysis after filtering all the homoeolog triads obtained from from ensembl.

**Supplementary Table S5: Expression profiles of genes/gene families involved in Strategy-II mode of Fe uptake.** Strategy-II components of Fe uptake were identified and classified based on screening wheat genes annotated by KOBAS for respective KO IDs for NAS, NAAT, YSL and DMAS genes.

**Supplementary Table S6: Expression profiles of genes/gene families involved in Strategy-I mode of Fe uptake.** Strategy-I components of Fe uptake were identified and classified based on screening wheat genes annotated by KOBAS for respective KO IDs for AHA, IRT, FRO, PEZ genes.

**Supplementary Table S7: Gene Ontology analysis of up- and down-regulated genes in response to Fe starvation.** WEGO tool was used to categorize DEGs into GO categories and identify significant GO terms. Table lists the number and percentage of up- and down-regulated genes as well as p-values for each GO term.

**Supplementary Table S8: Expression profiles of genes/gene of different transcription factors those are differentially up- and down regulated.** MapMan was used to identify TFs and categorize them into TF families. Table gives logFC value for starvation vs control for

each TF showing significantly altered expression. A gradient of red and green is used for up-regulated and down-regulated TFs respectively.

**Supplementary Table S9: Expression profiles of genes involved during the process of glutathione mediated detoxification process.** DEGs mapped to glutathione metabolism were identified using KOBAS. Table lists expression values and annotation for genes. Red color denotes up-regulated genes and green color represent down-regulation.

**Supplementary Table S10: GC-MS analysis of wheat roots subjected to 20 days of Fe starvation.** Each metabolite is represented with concentrations in three independent replicate manner. For concentration calculation, Individual metabolite area was normalized to sample weight and area of internal control (sorbitol). Metabolites with no detectable area in any of the conditions were considered to be the metabolite with minimum area. Delta method approximation was used to calculate standard errors (se) of log-ratio,  $se \log\text{-ratio} = 1/\ln 2 \sqrt{[(SET /T)^2 + (SEC /C)^2]}$ , where SET and SEC are standard errors of average  $-Fe$  and  $+Fe$  metabolite abundances. Metabolites with significant (p-value <0.05) differential abundance were plotted.

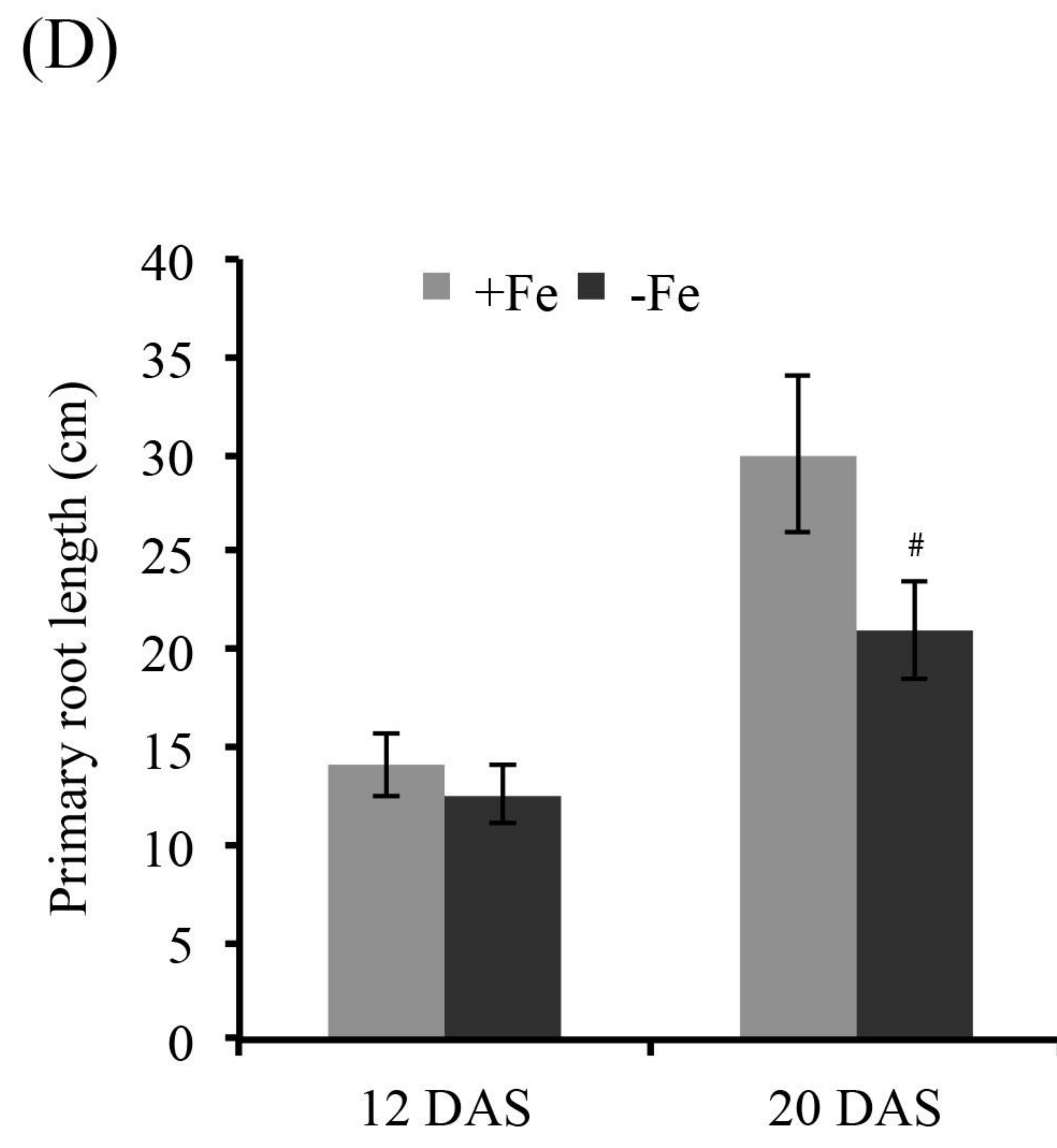
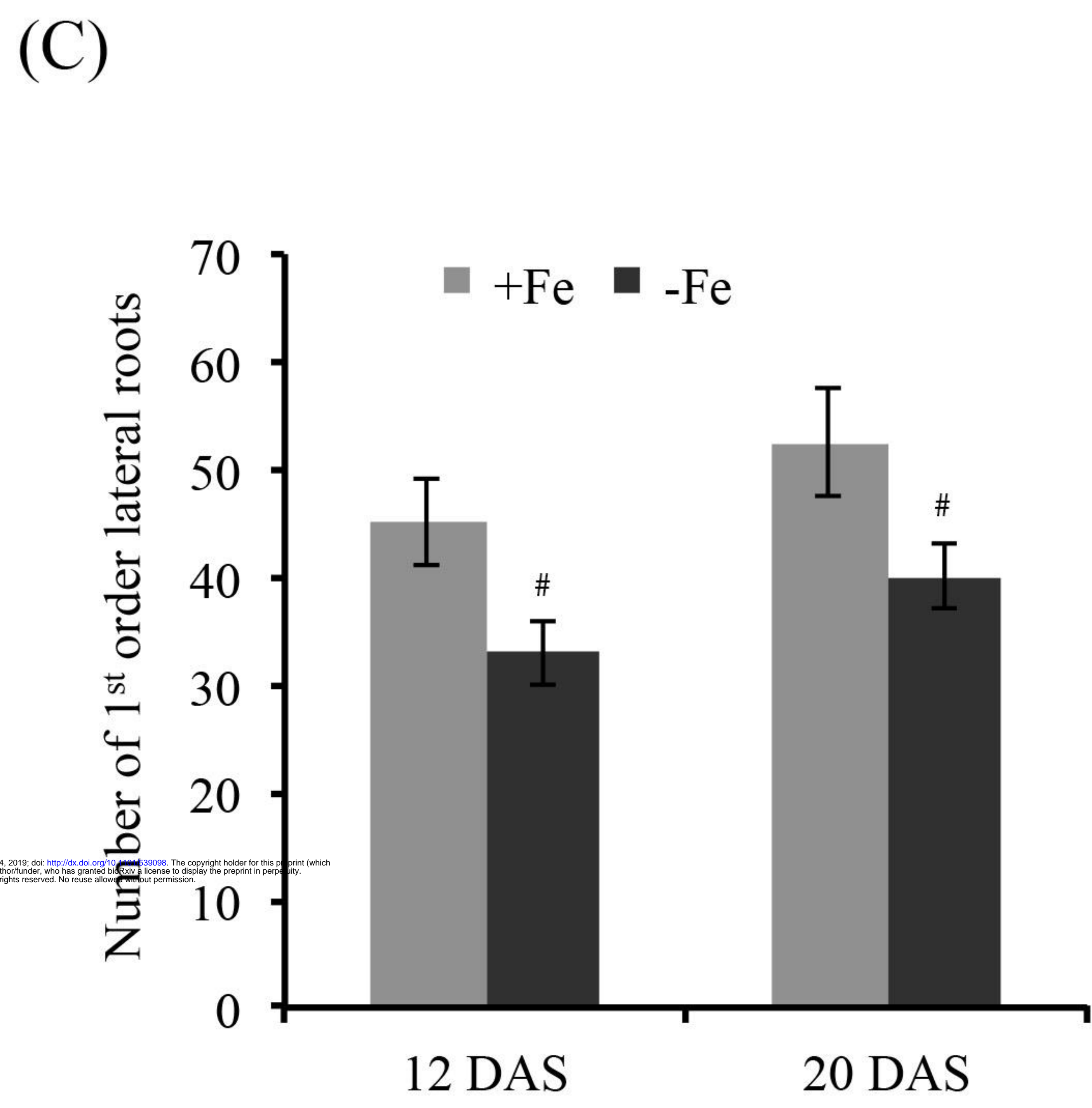
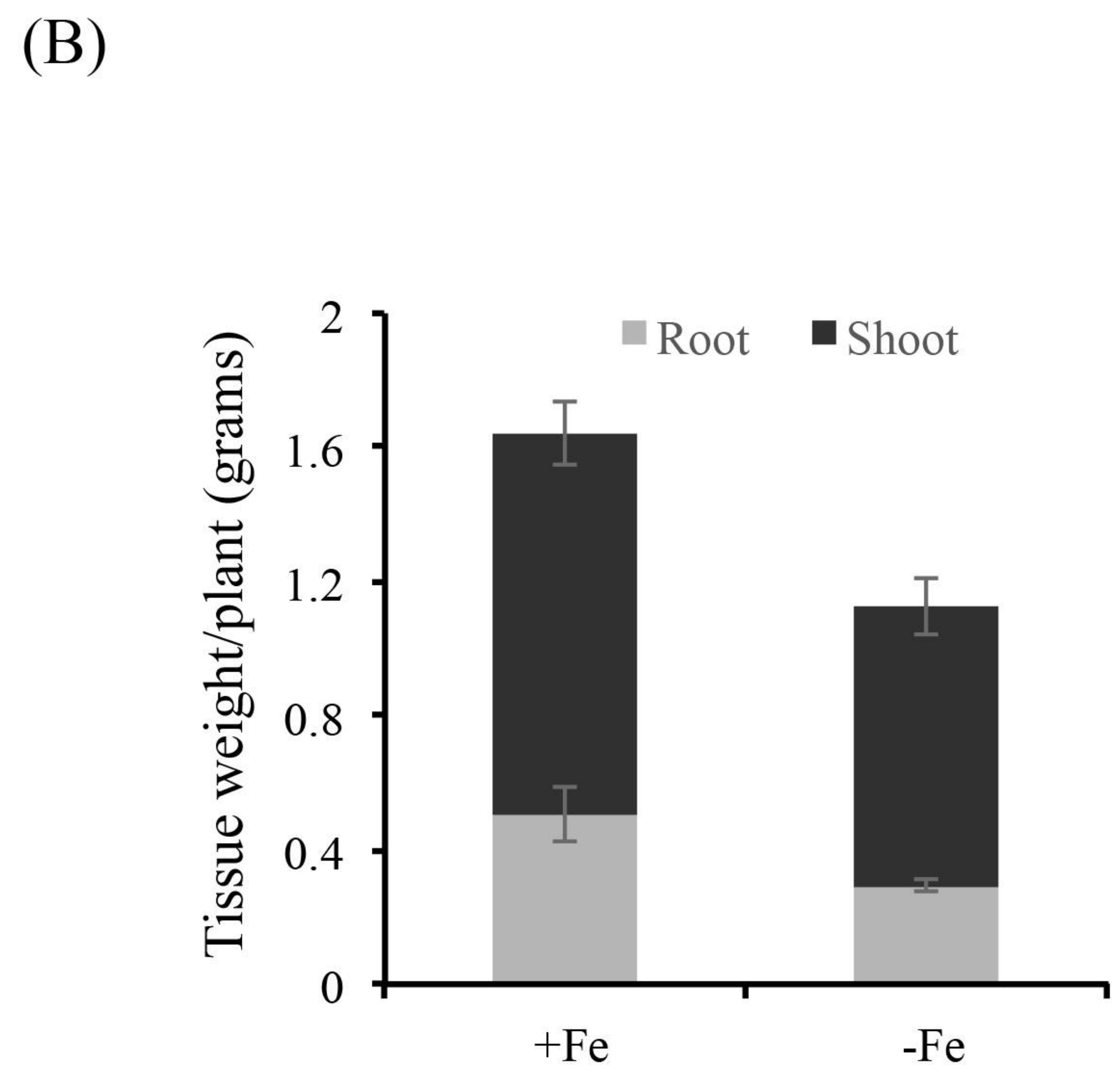
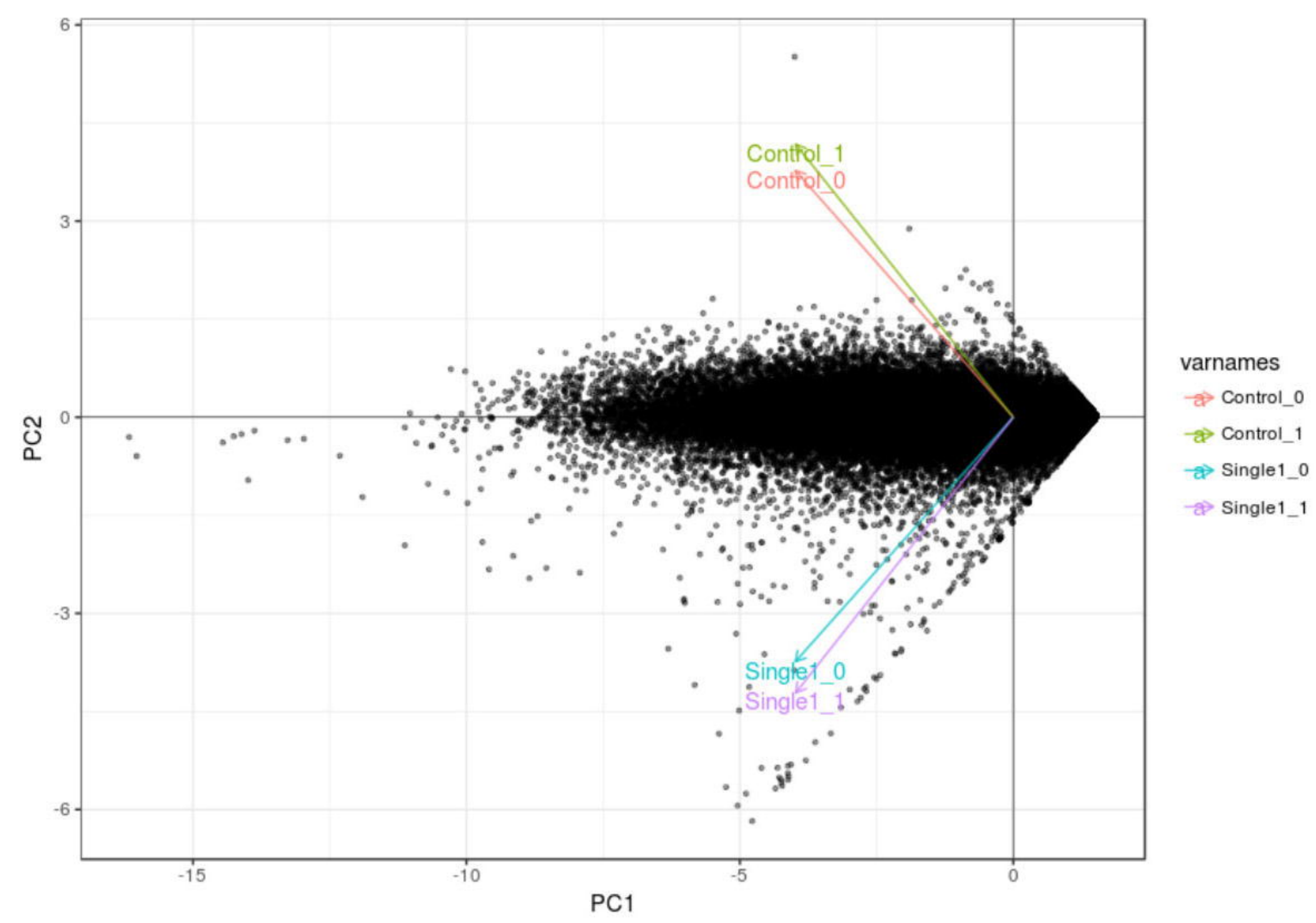
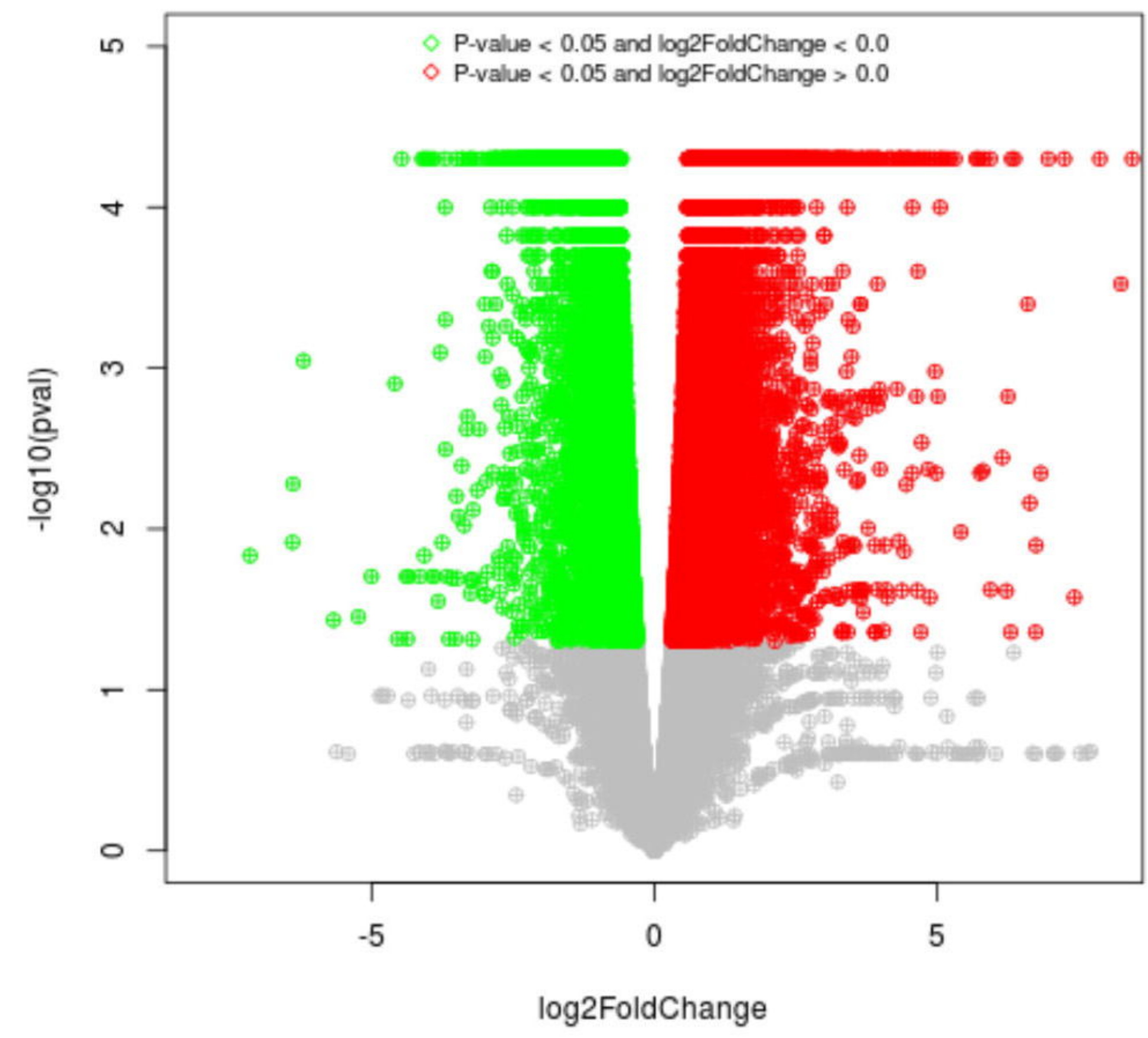


Figure 1

(A)



(B)



(C)

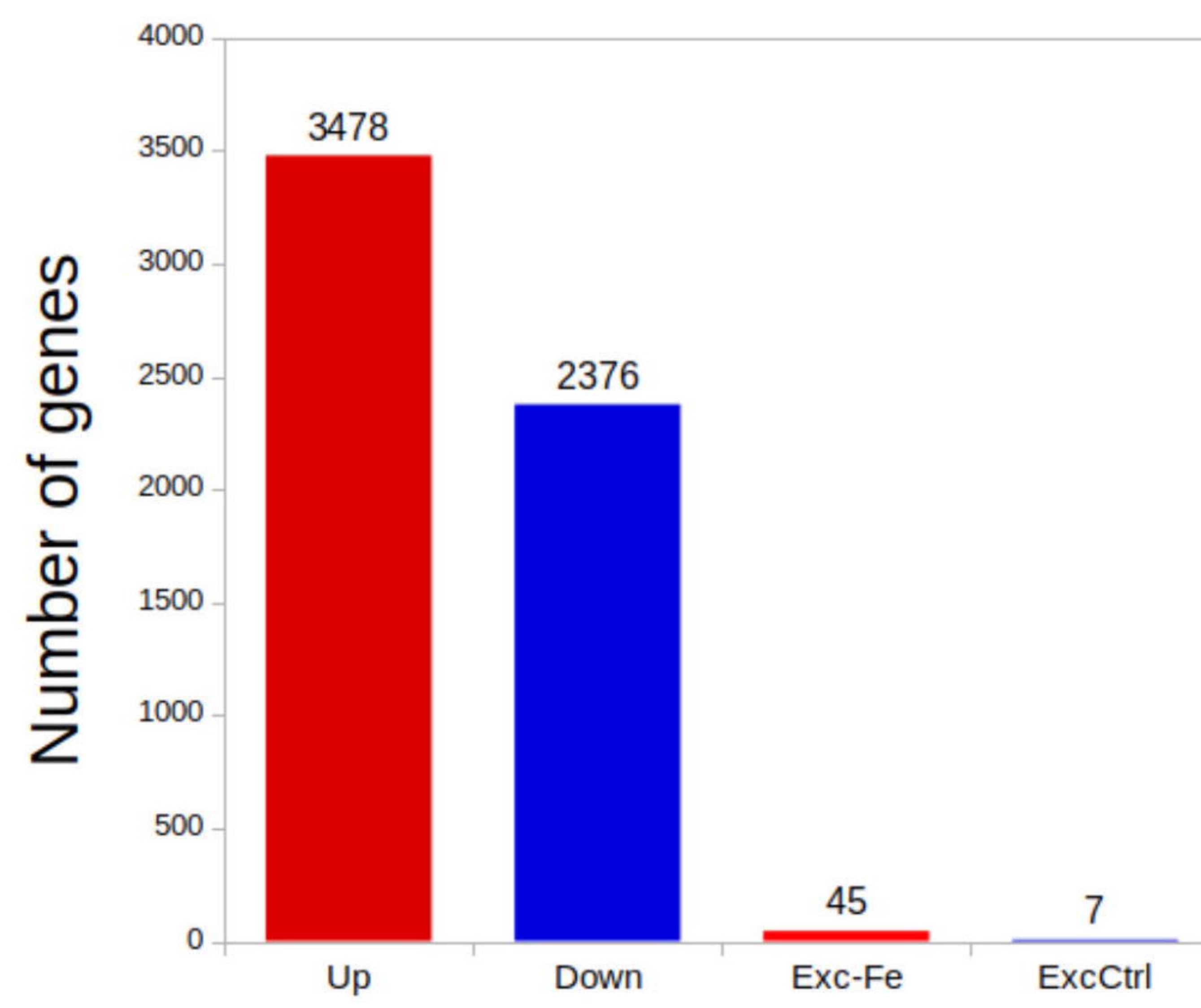
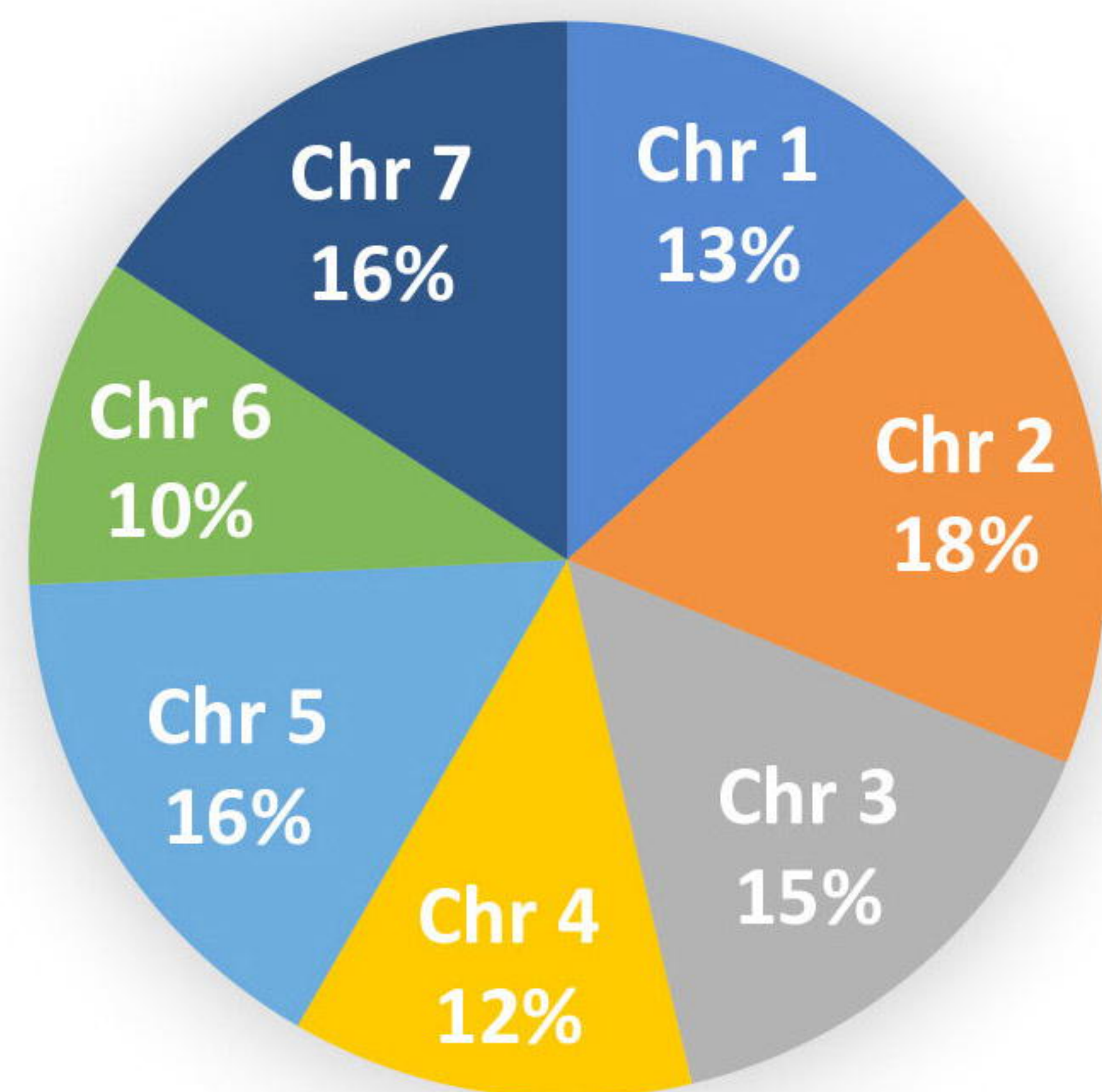
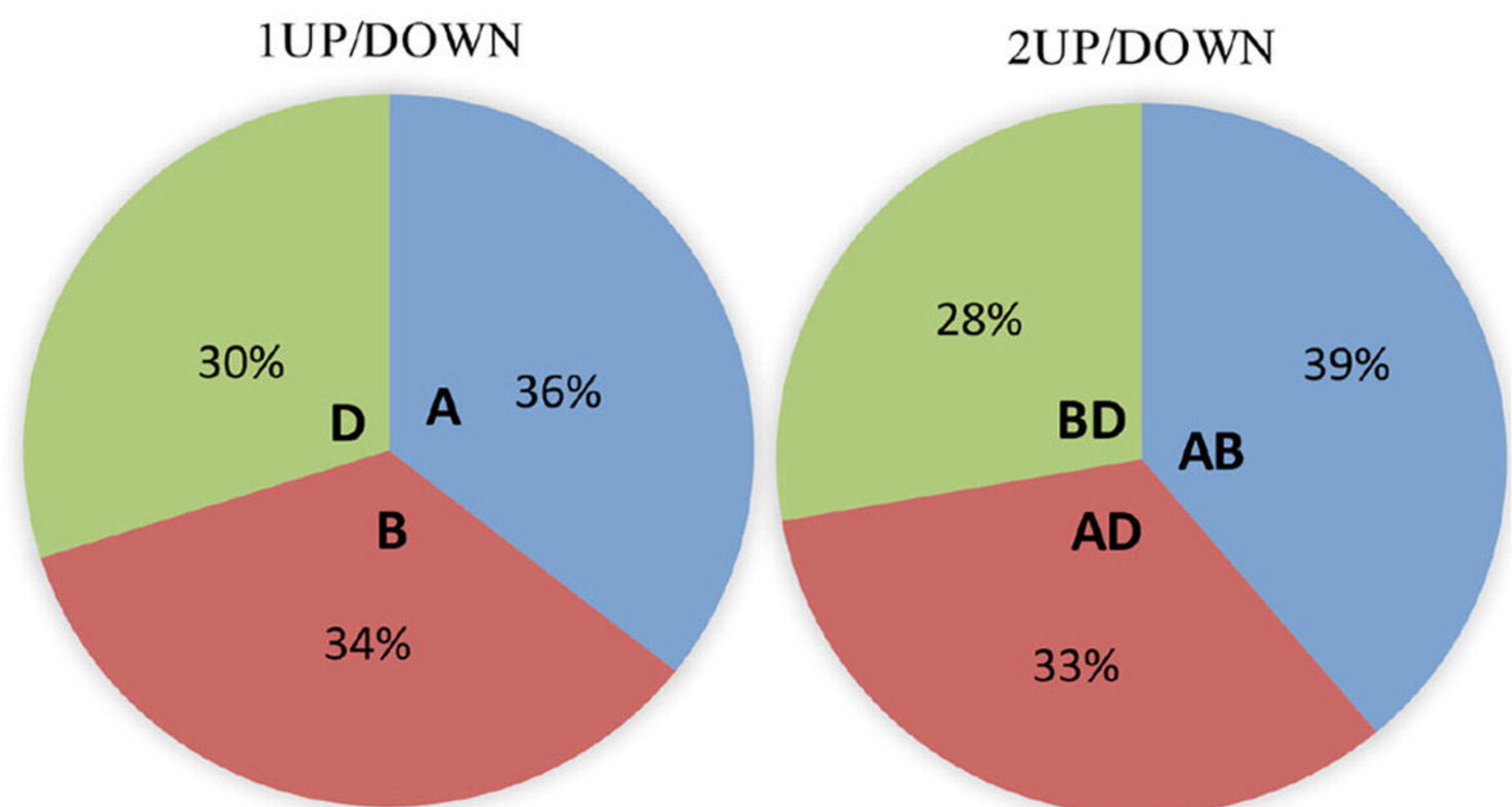


Figure 2

(A) -Fe DEGs distribution



(B)



(C)

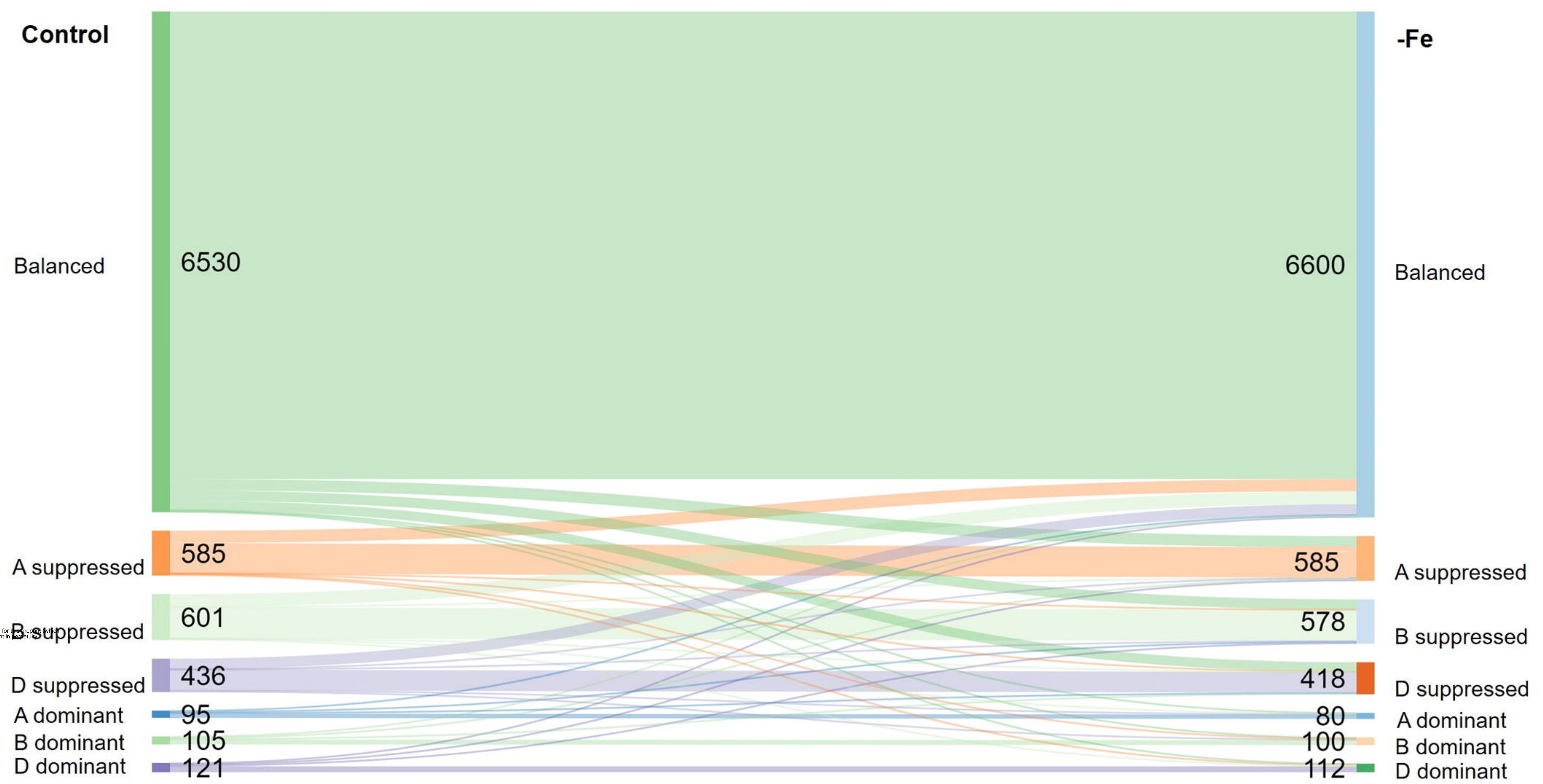


Figure 3

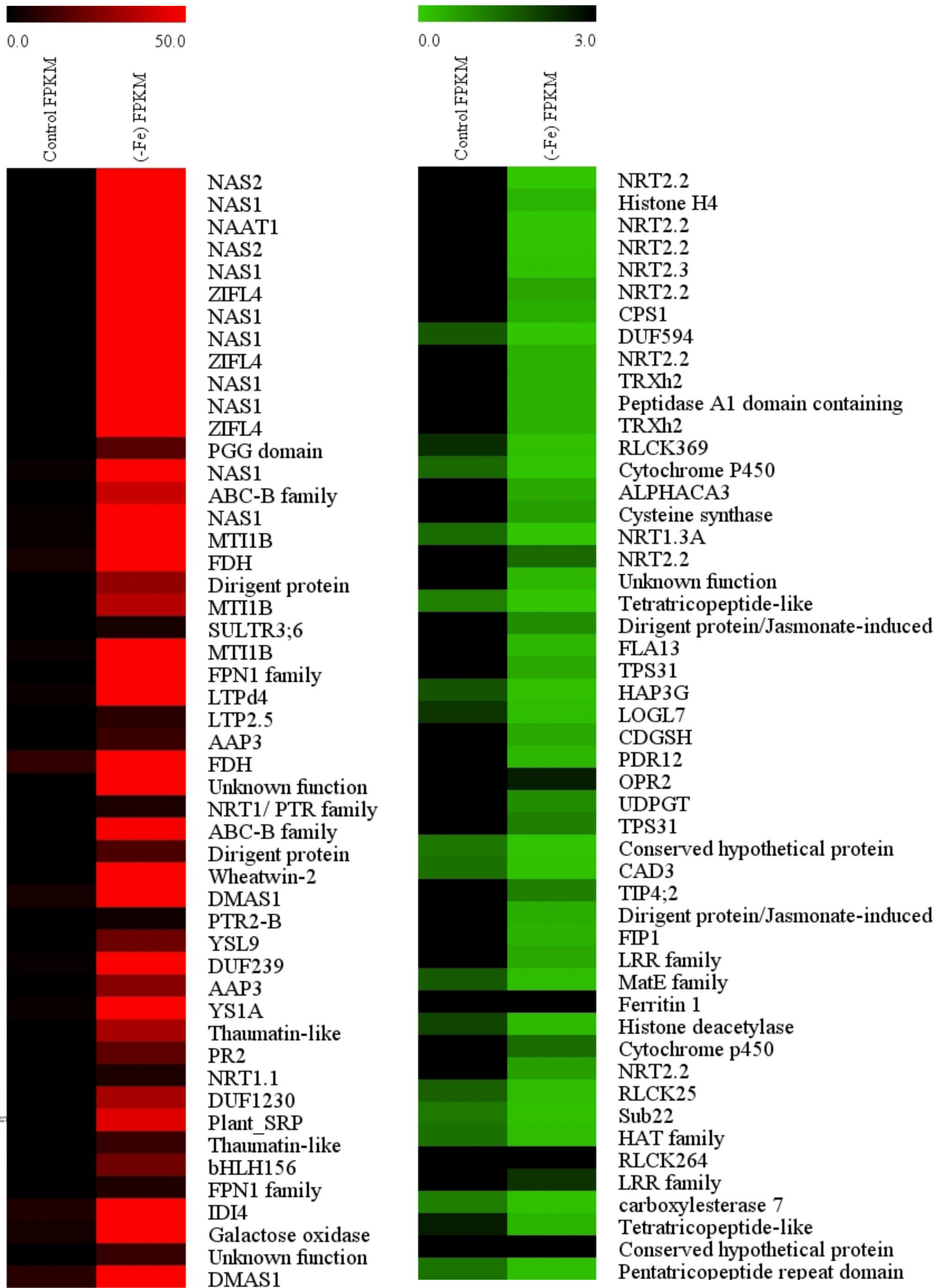
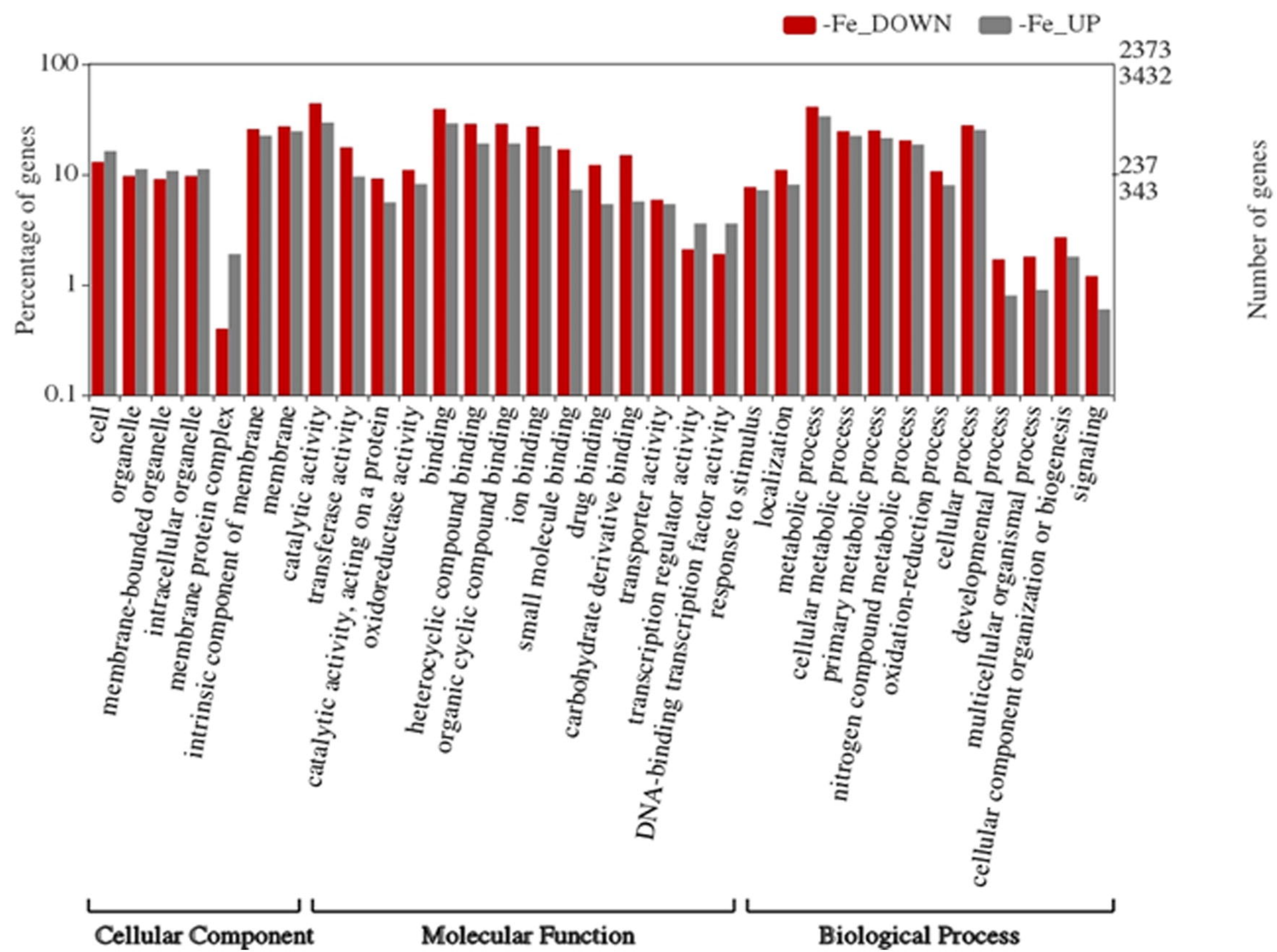
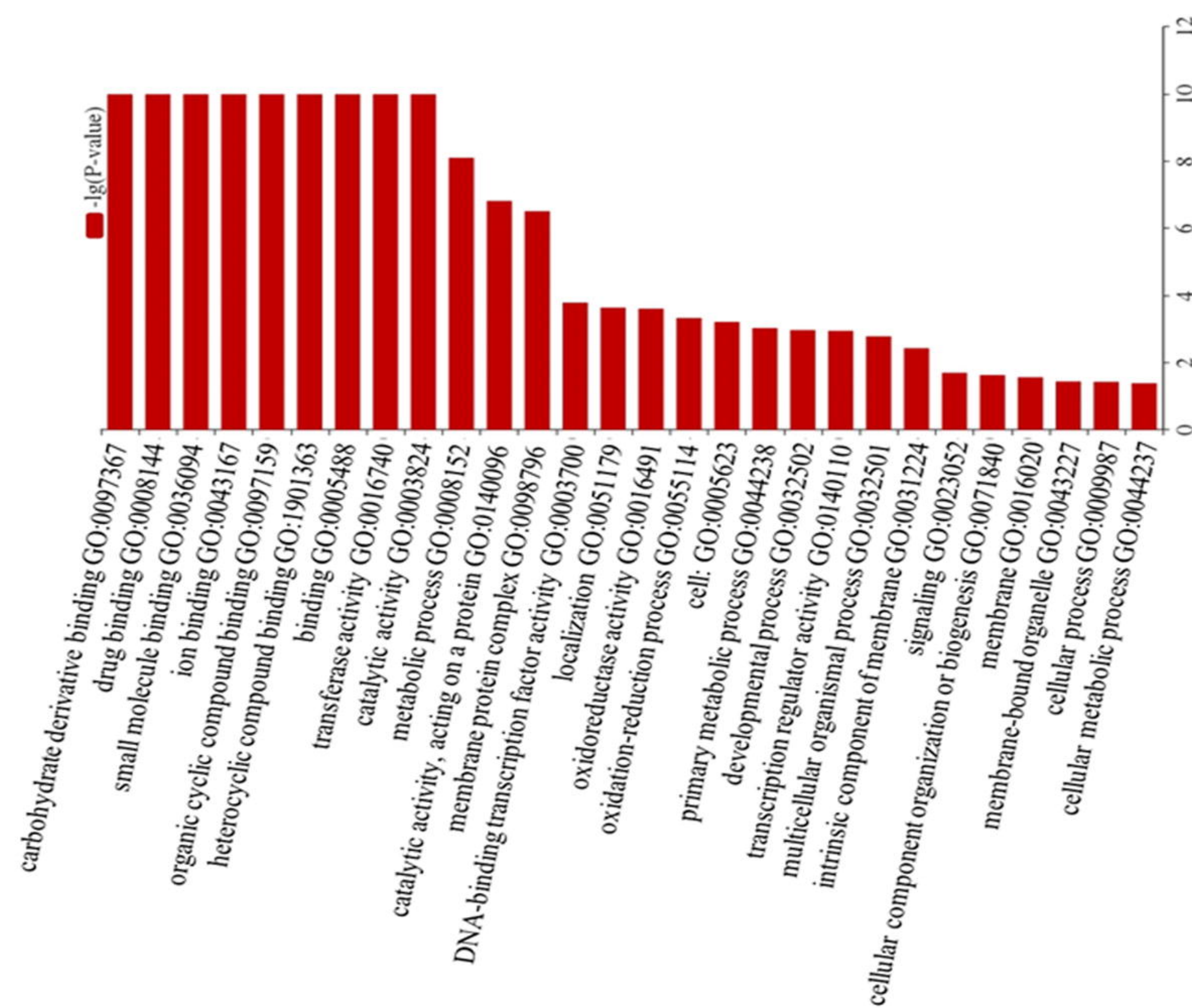


Figure 4

(A)



(B)



(C)

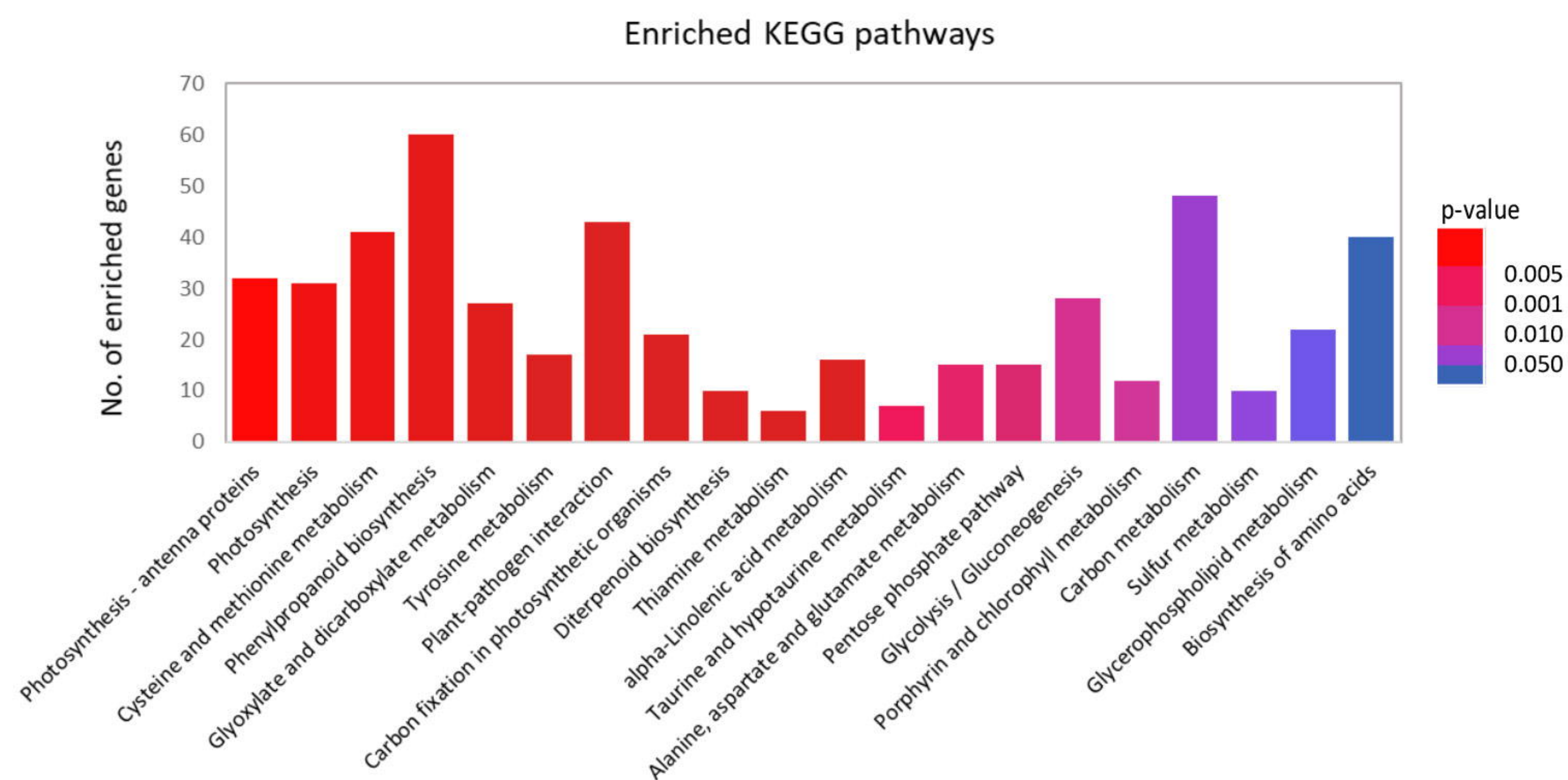
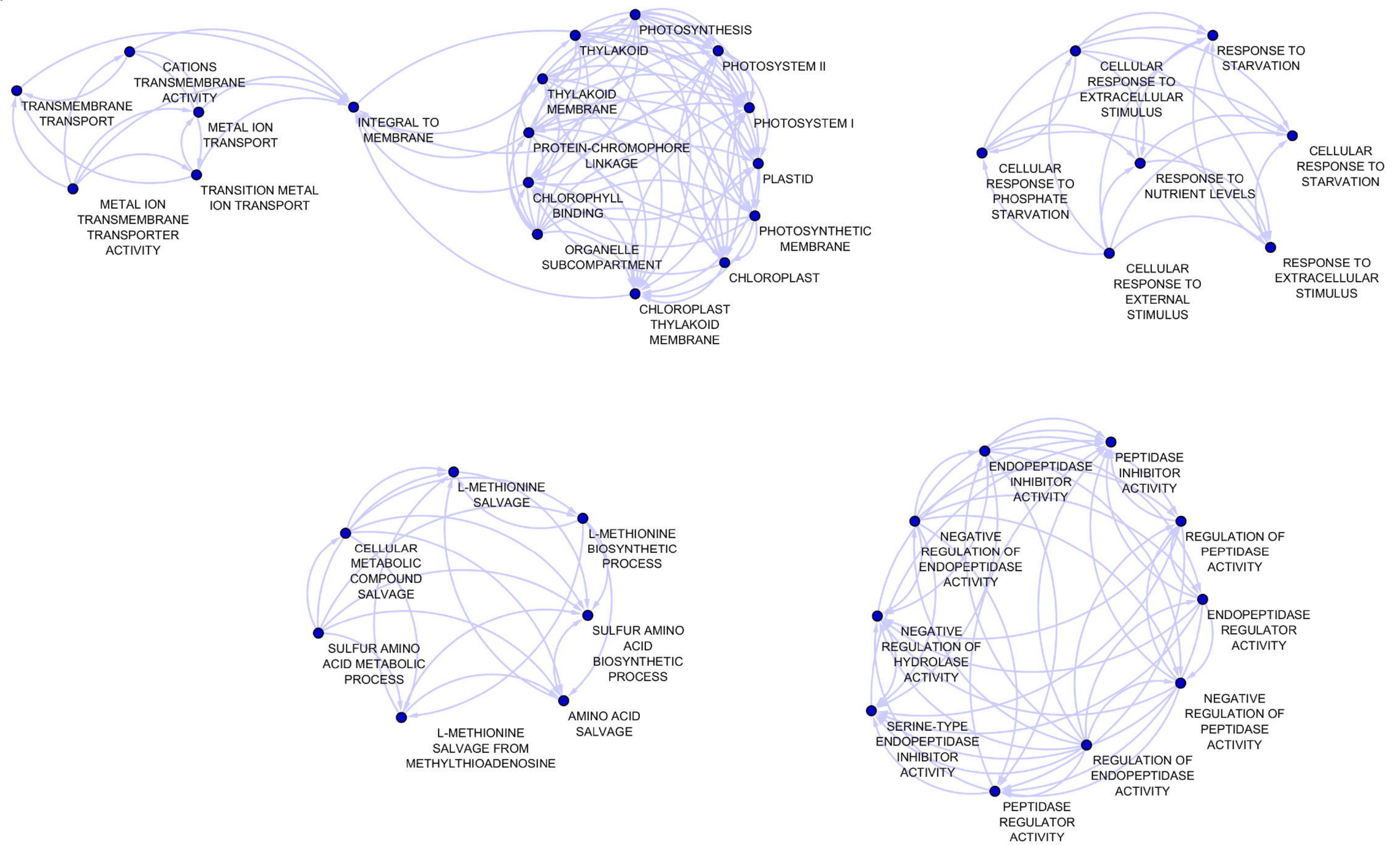
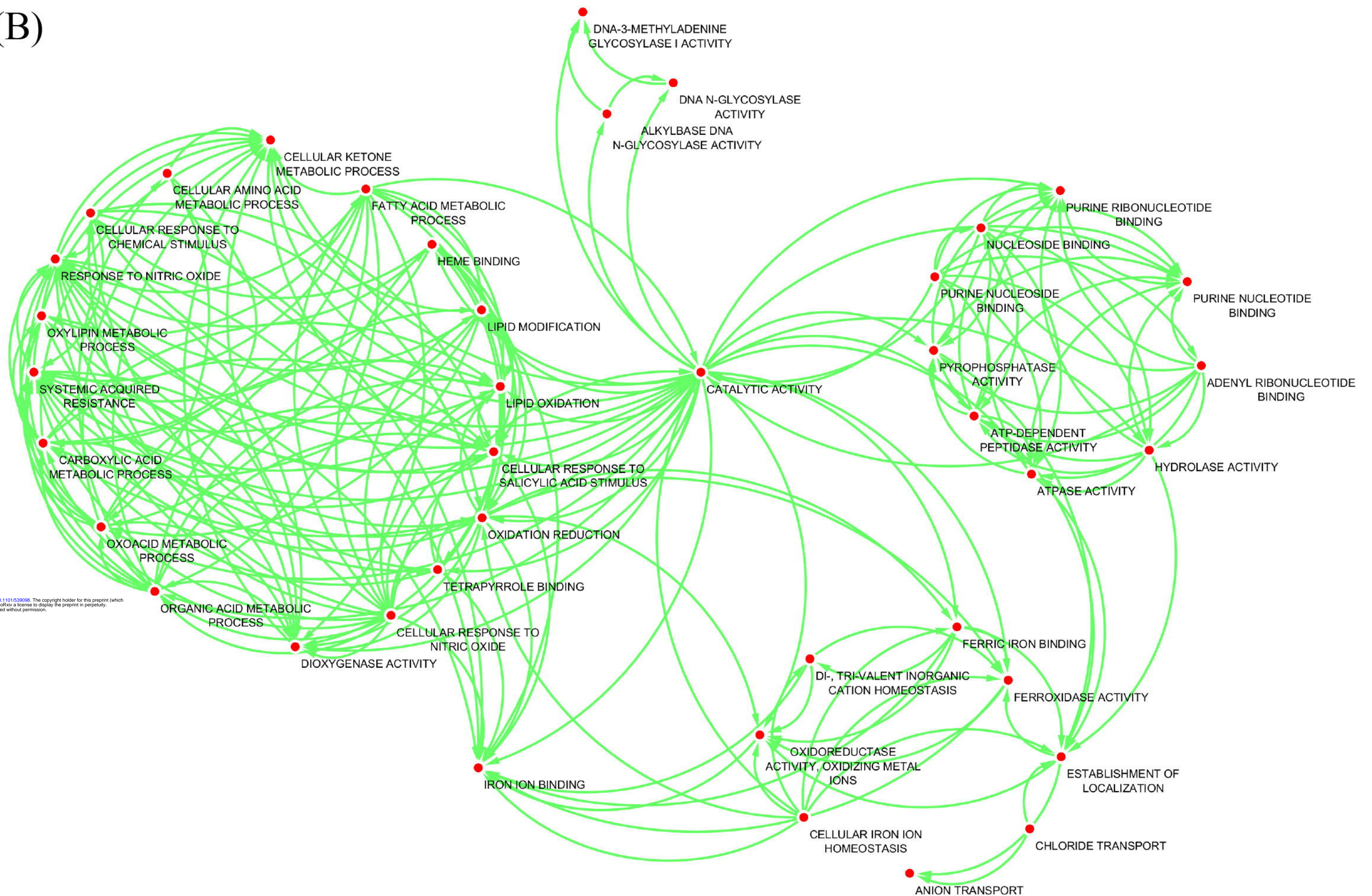


Figure 5

(A)



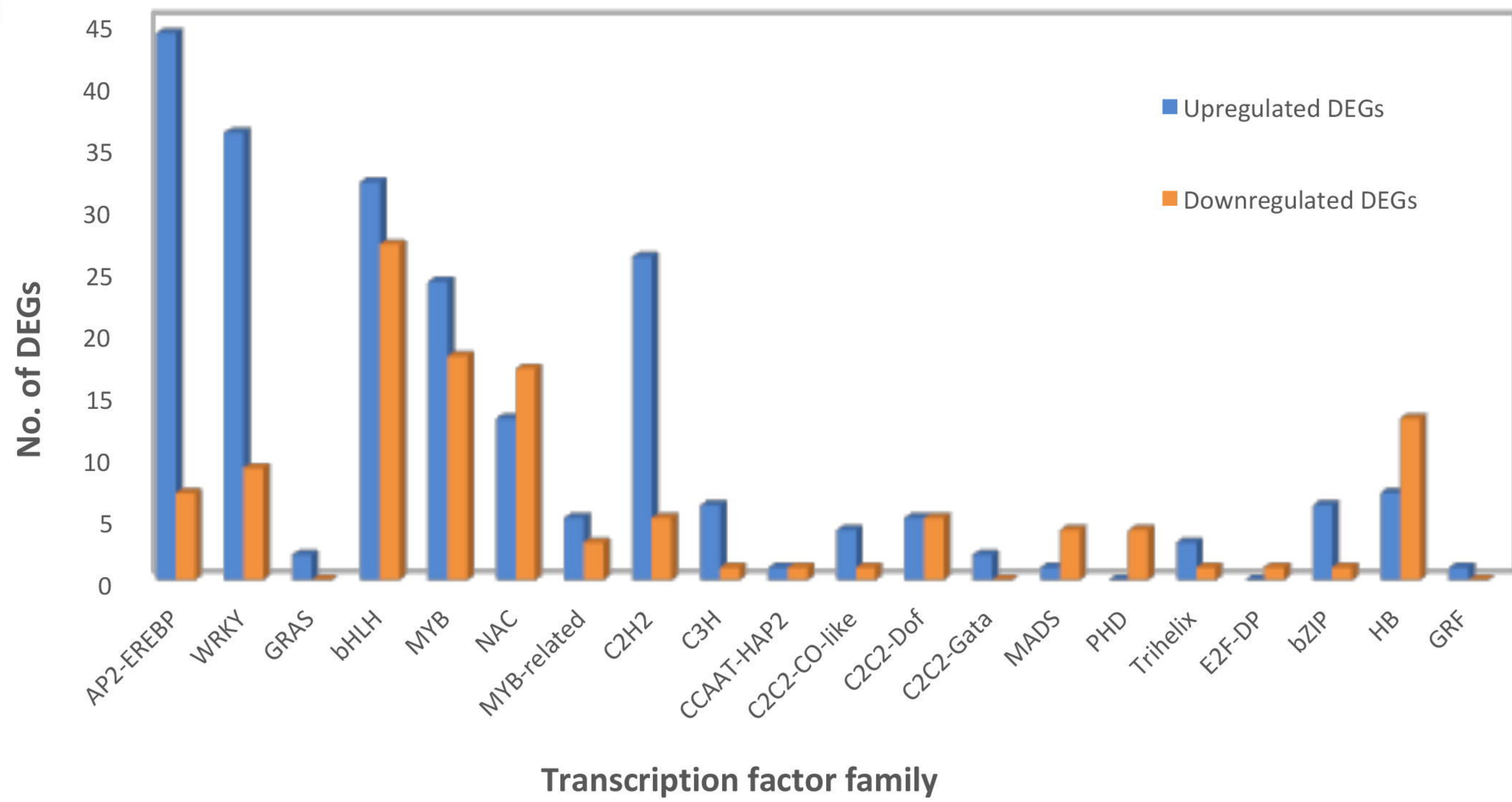
(B)



bioRxiv preprint first posted online Feb. 4, 2019; doi: <https://doi.org/10.1101/320098>. The copyright holder for this preprint (which was not peer-reviewed) is the author/funder, who has granted bioRxiv a license to display the preprint in perpetuity. All rights reserved. No reuse allowed without permission.

Figure 6

(A)



(B)

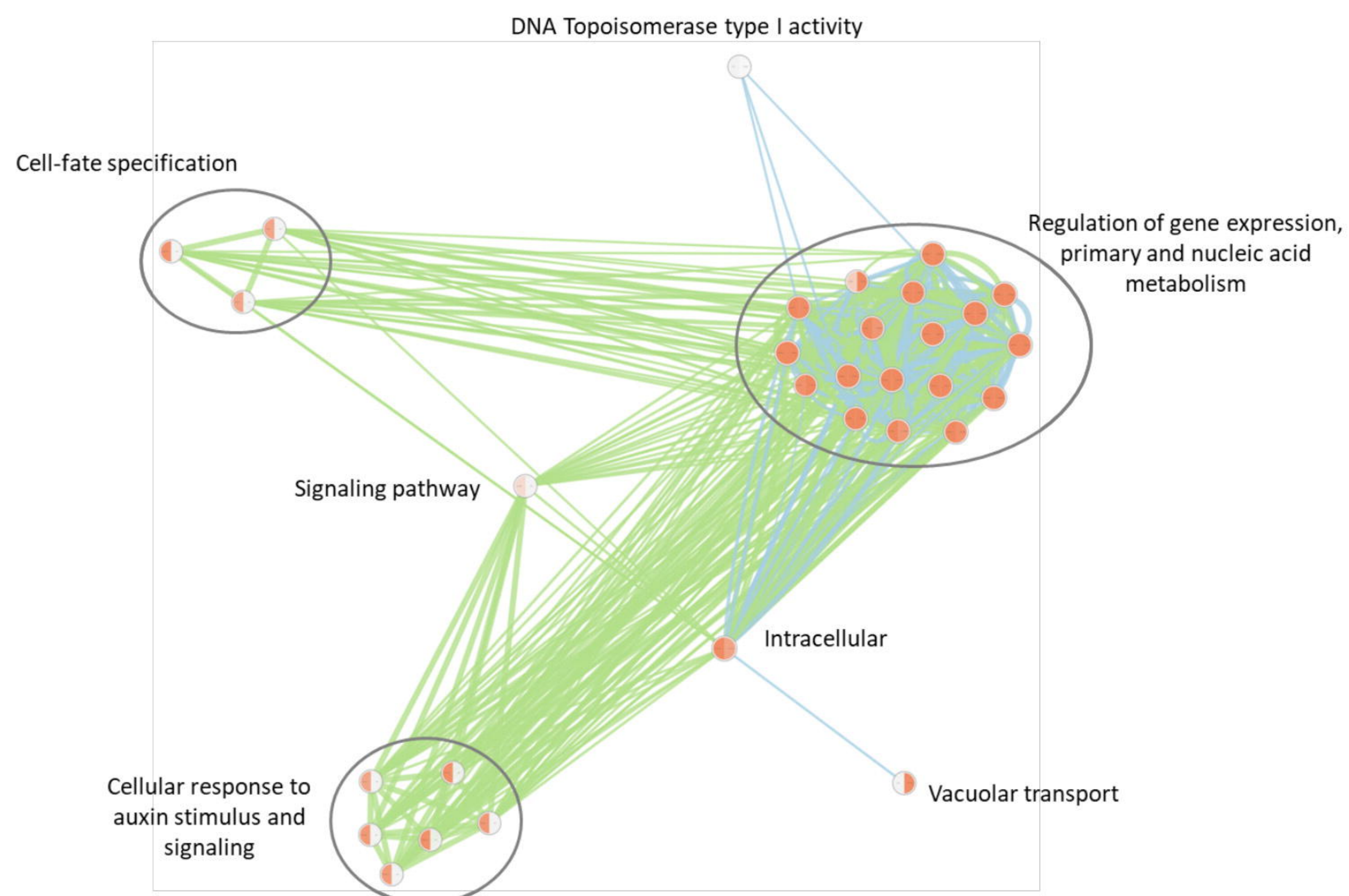
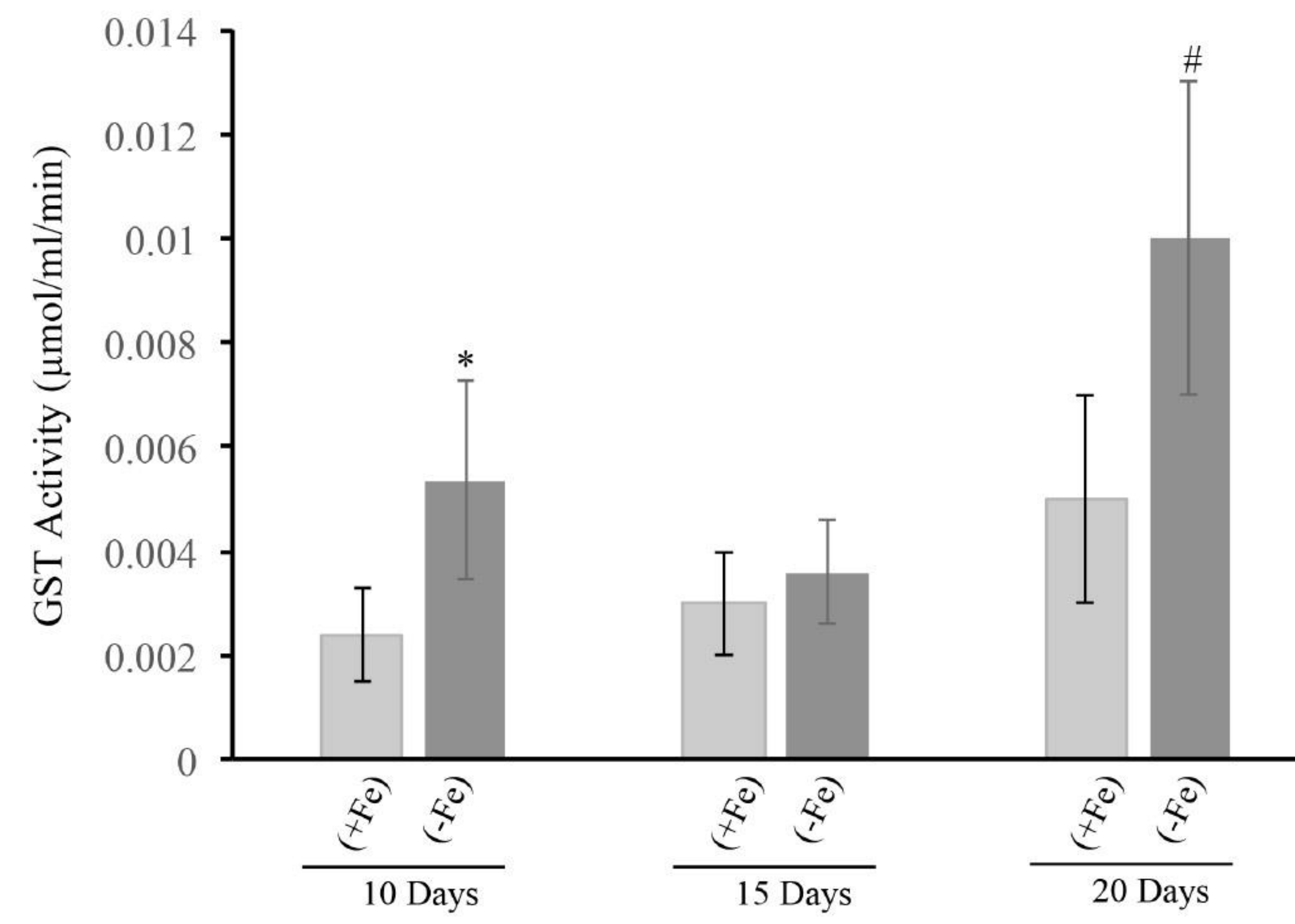


Figure 7

(A)



(B)

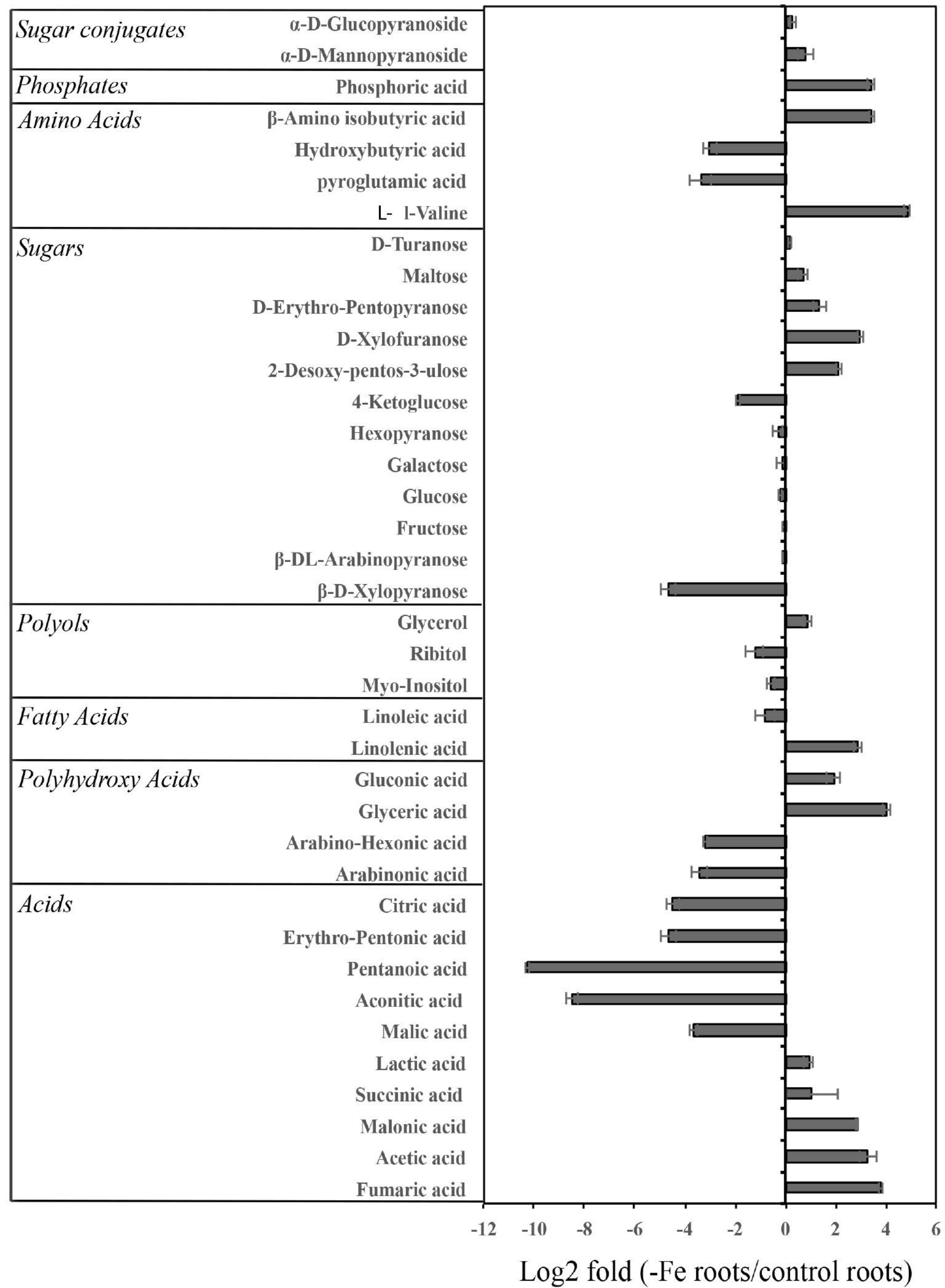
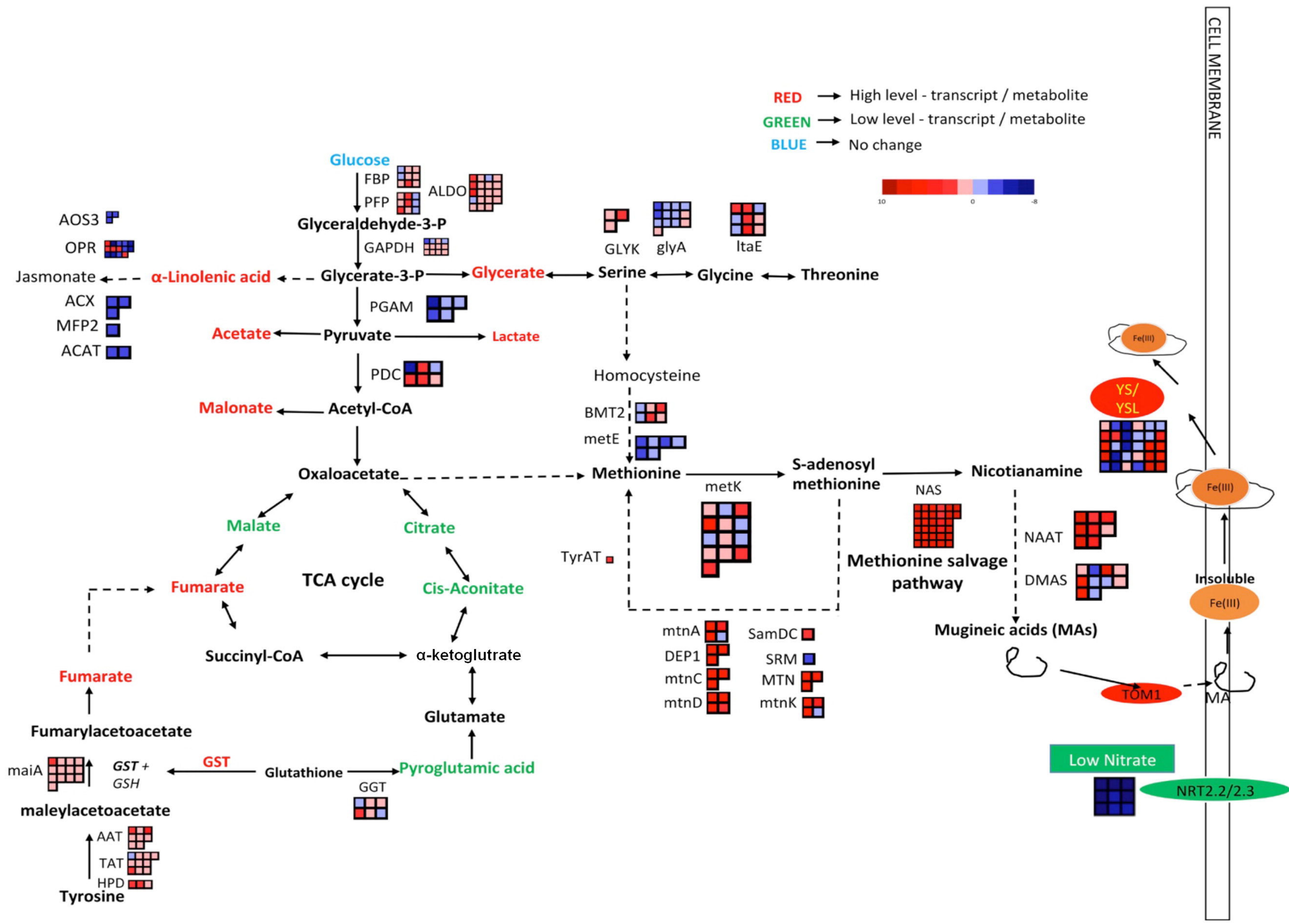


Figure 8



bioRxiv preprint first posted online Feb. 4, 2019; doi: <https://doi.org/10.1101/320098>. The copyright holder for this preprint (which was not peer-reviewed) is the author/funder, who has granted bioRxiv a license to display the preprint in perpetuity. All rights reserved. No reuse allowed without permission.

Figure 9